A mussel-inspired film for adhesion of wet buccal tissue and efficient buccal drug delivery

Shanshan Hu
State Key Laboratory of Oral Diseases, National Clinical Research Center for Oral Diseases Department of Prosthodontics, West China Hospital of Stomatology, Sichuan University, Chengdu, China.
Xibo Pei
Department of Prosthodontics, West China Hospital of Stomatology, Sichuan University, Chengdu, China
Lunliang Duan
National Engineering Research Center for Inland Waterway Regulation, Chongqing Jiaotong University, Chongqing, China.
Zhou Zhu
Department of Prosthodontics, West China Hospital of Stomatology, Sichuan University, Chengdu, China
Yanhua Liu
State Key Laboratory of Oral Diseases, National Clinical Research Center for Oral Diseases Department of Prosthodontics, West China Hospital of Stomatology, Sichuan University, Chengdu, China.
Junyu Chen
Department of Prosthodontics, West China Hospital of Stomatology, Sichuan University, Chengdu, China
Tao Chen
Stomatological Hospital of Chongqing Medical University
Ping Ji
Stomatological Hospital of Chongqing Medical University, Chongqing, China.
Qianbing Wan
Department of Prosthodontics, West China Hospital of Stomatology, Sichuan University, Chengdu, China
Jian Wang (ferowang@hotmail.com)
Department of Prosthodontics, West China Hospital of Stomatology, Sichuan University, Chengdu, China

Article

Keywords: buccal mucosa, drug bioavailability, oral mucositis models

Posted Date: September 9th, 2020

DOI: https://doi.org/10.21203/rs.3.rs-69144/v1

Version of Record: A version of this preprint was published at Nature Communications on March 16th, 2021. See the published version at https://doi.org/10.1038/s41467-021-21989-5.

A mussel-inspired film for adhesion of wet buccal tissue and efficient buccal drug delivery

Shanshan Hu[1,2], Xibo Pei[1,3], Lunliang Duan[4], Zhou Zhu[1,3], Yanhua Liu[1], Junyu Chen[1,3], Tao Chen[2], Ping Ji[2], Qianbing Wan[1,3*], Jian Wang[1,3*]

[1]State Key Laboratory of Oral Diseases, National Clinical Research Center for Oral Diseases Department of Prosthodontics, West China Hospital of Stomatology, Sichuan University, Chengdu, China. [2]Stomatological Hospital of Chongqing Medical University, Chongqing Key Laboratory of Oral Diseases and Biomedical Sciences, Chongqing Municipal Key Laboratory of Oral Biomedical Engineering of Higher Education, Chongqing, China. [3]Department of Prosthodontics, West China Hospital of Stomatology, Sichuan University, Chengdu, China. [4]National Engineering Research Center for Inland Waterway Regulation, Chongqing Jiaotong University, Chongqing, China.

These authors contributed equally: Shanshan Hu, Xibo Pei.

*Corresponding Authors. e-mail: champion@scu.edu.cn; ferowang@hotmail.com.

Administration of drug via the buccal route has attracted much attention in recent years. However, developing system with satisfactory adhesion in wet conditions and drug bioavailability still remains a challenge. Here, we propose a mussel inspired mucoadhesive film. Ex vivo porcine and in vivo rat models show that the film can achieve strong adhesion with wet buccal tissues. We also demonstrate that the film exhibits tunable mucoadhesion strength and erosion rate. The adhesion mechanism of this film relies on both physical association and covalent bonding between the film and mucus. Then, polydopamine (PDA) modified nanoparticles (NPs) are incorporated into the film and the PDA NPs loaded films show superior advantages to transport across multiple barriers of buccal mucosa with improved drug bioavailability and therapeutic efficacy in oral mucositis models. We anticipate that this platform might aid the development of tissue adhesives and inspire the design of nanoparticle-based buccal delivery systems.

Every day, millions of patients across the globe are subjected to undesirable side-effects caused by high dosages of drugs via oral route[1] or a fear of injections[2]. An estimated of over 80% patients are suffering from severe needle phobia[2]. Buccal drug delivery, which is non-invasive, painless and convenient, offers superb advantages over the oral and parenteral formulations[1]. By avoiding enzymatic degradation in the gastrointestinal tract as well as first-pass hepatic metabolism[3-5], delivery of drugs via buccal mucosa would markedly improve patient experience and disease outcomes. However, there are also many challenges facing this route that have limited its further implementation. Thus, developing formulations with improved therapeutic effect is a major unmet clinical need for effective buccal drug delivery.

The main challenge related to the buccal route is the residence time[6]. To ensure optimal drug efficiency, buccal drug delivery formulations need to maintain an intimate contact with the oral mucosa for a long period of time. However, flushes of saliva, swallowing, and mouth movement could all influence the residence time of formulation in buccal cavity[4,5,7]. Therefore, achieving strong adhesion in the wet conditions of oral cavity is challenging. Current existing tissue adhesives are subjected to several limitations, including weak bonding, poor mechanical match with tissues, slow adhesion formation, and low biological compatibility[8-11]. Meanwhile, the buccal administration routes have substantial transport barriers. Drugs must diffuse the mucus layer that covers the surface of oral mucosa and transport across the epithelial layer to be absorbed[12-14]. Unfortunately, despite the overwhelming clinical need for optimum buccal drug delivery, few formulations that exhibit excellent properties to overcome these limitations have yet been reported.

On the basis of these limitations, the ideal buccal drug delivery systems should exhibit the following properties: (1) strong adhesion in wet environment to enable enough residence time; (2) tunable size and thickness and high elasticity to be capable of mechanically matching tissues; (3) ability to transport across the epithelial barriers; (4) controlled and prolonged drug release profile; and (5) a high degree of biocompatibility. Therefore, tempts should be made to develop drug delivery systems encompassing these characteristics. Mussel, which is well known for its remarkable underwater adhesion ability in addition to its biocompatibility, is a potential ideal tissue adhesive in the biological field[15-19]. In addition, nanoparticles (NPs) have shown superb advantages on improved navigation through the mucus and epithelium barrier and could be tuned to display a controlled or sustained release behavior[20-23]. Therefore, the use of

strong tissue adhesive combined with NPs as drug carriers is a good strategy to overcome the limitations associated with buccal administration route.

Here, we propose a novel buccal tissue adhesive in the form of tunable thin film made from a combination of mucoadhesive polymer poly(vinyl alcohol) (PVA) and mussel adhesive protein 3,4-dihydroxy-D-phenylalanine (DOPA) (PVA-DOPA film). Ex vivo porcine and in vivo rat models show that the film can achieve strong adhesion and match well with wet buccal tissues. We also demonstrate that the film exhibit tunable mucoadhesion strength and erosion rate in proportion to the amount of DOPA. The adhesion mechanism of this film relies on the physical interpenetration and the formation of hydrogen bonds between polymer chains and the mucus in the initial phase, resulting in fast temporary crosslinking with the buccal tissue. Subsequent covalent crosslinking of catechol groups with the amino or thiol groups of the tissue further improves the adhesion stability and strength of the film. Then, we adopt three kinds of polymers (poly(ethylene glycol), PVA, dopamine) to assemble core-shell poly(lactic-co-glycolic acid) (PLGA) NPs with different surface coatings (Fig. 1a) and incorporated them into the PVA-DOPA film to form a combined buccal drug delivery system (PVA-DOPA@NPs film), as shown schematically in Fig. 1b. Through systematical evaluation, we observe that the polydopamine (PDA) modified NPs exhibit good mucus-penetrating abilities and are more readily transported across the epithelia cells (Fig. 1c). The anti-inflammatory drug, dexamethasone (Dex), is chosen as model compounds to establish the release behavior of the film. The results show that the buccally administered film incorporated with drug-loaded PLGA-PDA NPs show the best bioavailability and superb therapeutic efficacy for oral mucositis. Therefore, we present a novel integrated buccal drug delivery system, in which NPs show controlled drug release profile, improved mucus-penetrating ability and cellular uptake, while the shielding film shows prolonged residence time and improved mucoadhesion.

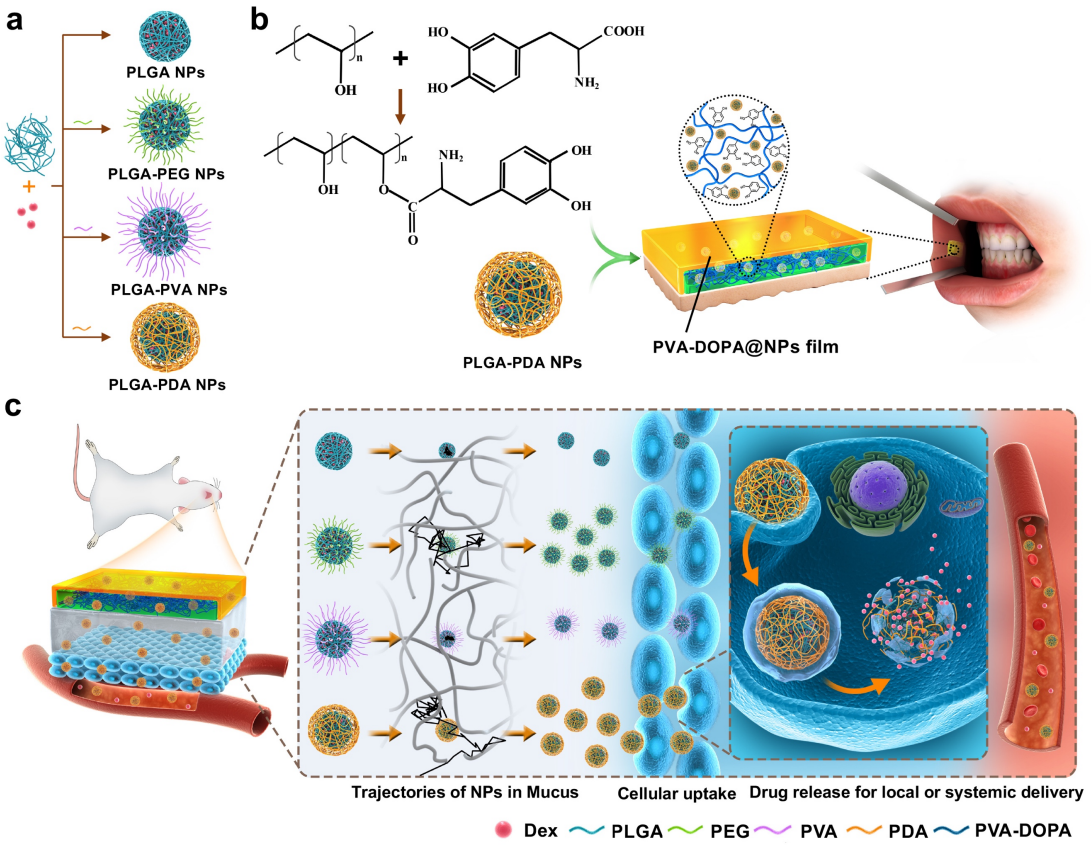

Fig. 1 Synthesis and biomedical application of PVA-DOPA@NPs-Dex mucoadhesive film. a Illustrations displaying the method to assemble core-shell PLGA NPs with different surface modifications. **b** Schematic presentation of fabrication of the PVA-DOPA@NPs-Dex film with enhanced mucoadhesion for buccal drug delivery. **c** Schematic diagram of application of PVA-DOPA@NPs-Dex film on rat buccal mucosa and the process of the NPs to sequentially permeate the mucus layer and the epithelia cells. PDA coated PLGA NPs could overcome both barriers rapidly and subsequently release drug for local or systemic delivery. Dex: dexamethasone, PLGA: poly(lactic-co-glycolic acid), PEG: poly(ethylene glycol), PVA: poly(vinyl alcohol), PDA: polydopamine, DOPA: 3,4-dihydroxy-D-phenylalanine.

Results

Preparation and characterization of the PVA-DOPA mucoadhesive film. The schematic diagram for the fabrication of the PVA-DOPA mucoadhesive film was presented in Fig. 1b. Firstly, by esterification reaction, PVA-DOPA polymers were synthesized by modifying PVA with mussel adhesive protein 3,4-dihydroxy-D-phenylalanine (DOPA). The formation of PVA-DOPA1-6 (according to the content of DOPA added, refer to the Material section) was confirmed by Fourier transform infrared (FTIR) (Supplementary Fig. 1a), ultraviolet-visible (UV-vis) (Fig. 2a), and ^{1}H-nuclear magnetic resonance (^{1}H-NMR) spectra (Fig. 2b). The existence of vibration absorption peak (1734 cm^{-1}) for the C=O bond proved the successful synthesis of PVA-DOPA polymers (Supplementary Fig. 1a). In addition, the absorption peaks of catechol in the UV-vis (280 nm) (Fig. 2a) and the ^{1}H-NMR spectra (6.5-6.8 ppm) (Fig. 2b) also

demonstrated that the PVA-DOPA polymers were successfully synthesized, and the extent of absorption peaks were in proportional to the amount of added DOPA. Supplementary Table 1 also showed the grafting percentage of different PVA-DOPA, as the result indicated, the grafting rate ranged from 65.0% to 83.3%. The photograph of the ethyl cellulose protective cap, lyophilized PVA-DOPA film and film after hydration were respectively presented in Supplementary Fig. 1b-1e. Additionally, the thickness and surface pH of different PVA-DOPA were presented in Supplementary Table 2. As shown, the thickness uniformity assured dose accuracy of the prepared film formulations and the near neutral surface pH indicated no potential irritation to the mucosa.

Then the results of rheological studies (Fig.2c and 2d) verified the formation of covalently cross-linked networks[24], however, the crosslinking density of the networks decreased with increase of the amount of DOPA, perhaps due to the readily self-crosslinking properties of the DOPA molecules[25,26]. Furthermore, the tensile strength and strain testing demonstrated good breakability and flexibility behavior of the films (Supplementary Fig. 1f-h) and indicated their ability to accommodate well with the outline of the buccal cavity after application, capable of mechanically matching soft tissues[27]. Swelling assessment is essential to understand the mucoadhesive properties as well as the release rate of drugs incorporated in films[28,29]. As the results indicated, all the prepared PVA-DOPA films showed sufficient hydration to form adhesion with the buccal mucosa and the rate of hydration was rapid in the initial phase of around 2 h (Supplementary Fig. 1i). However, it is not wise to compare the hydration rate of each PVA-DOPA film since it was also clearly seen that the extent of erosion increased progressively with the content of DOPA (Fig. 2e). Therefore, the hydration rate of PVA-DOPA5 and PVA-DOPA6 decreased rapidly after 4 h, due to their higher erosion rate (Fig. 2e). The reduction in the crosslinking density of the film likely hastened the rate of degradation of PVA-DOPA film with high content of DOPA. Hence, the erosion rate of the film can be controlled over time periods from several hours to several days by tuning its composition and this DOPA related tunable erosion rate of the PVA-DOPA films also makes it potential to be applicable to various kinds of diseases which demand different dosage intervals.

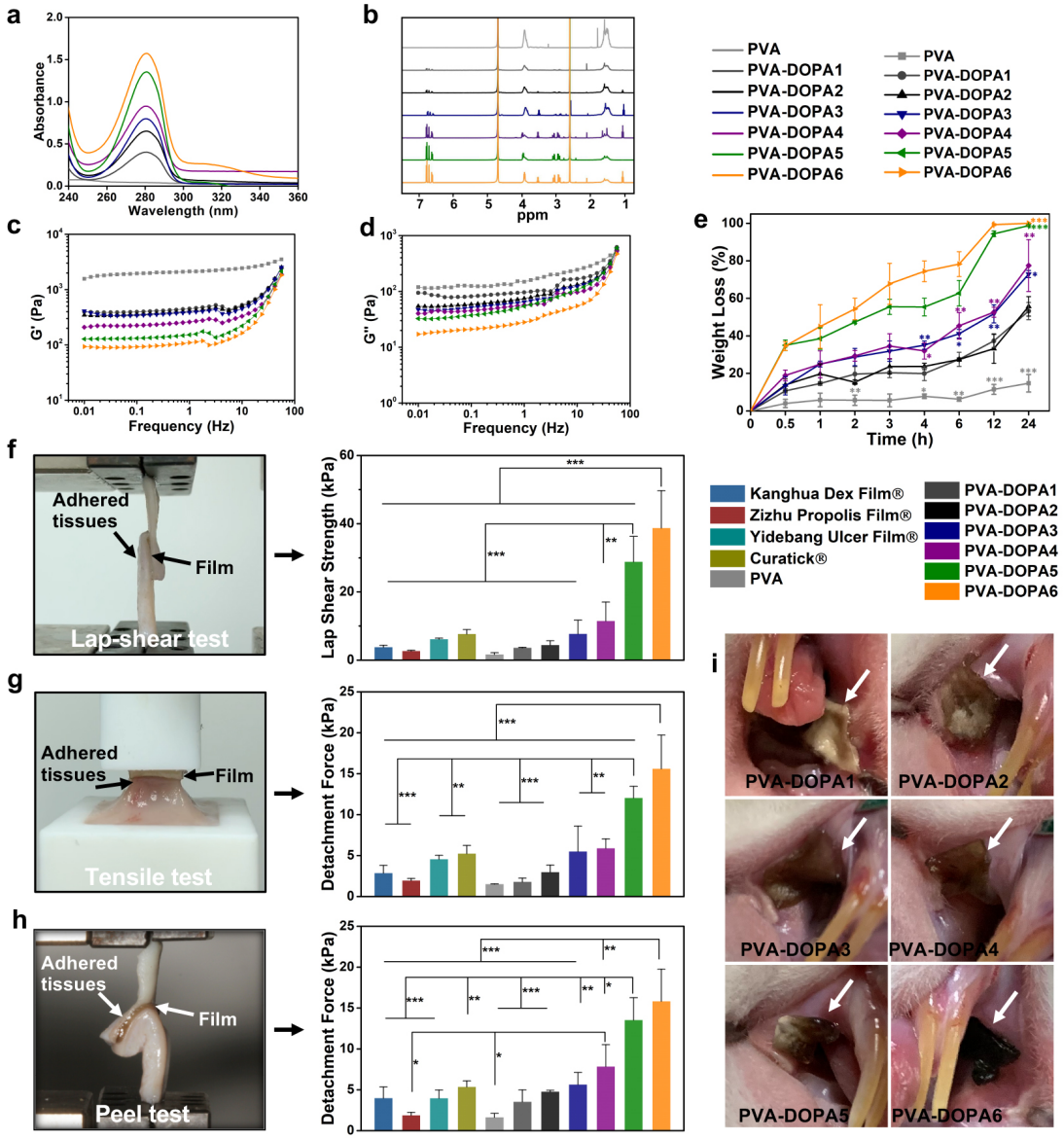

Fig. 2 Characterization and adhesion strength of PVA-DOPA films. a UV-vis absorbance spectrum of PVA-DOPA polymers with different amount of DOPA. **b** ^{1}H-NMR spectra of PVA-DOPA polymers with different content of DOPA. **c** Storage (G′) moduli of films with different content of DOPA. **d** Loss (G″) moduli of films with different content of DOPA. **e** Erosion rate of films with different content of DOPA as a function of time **f** Comparison of shear strength of PVA-DOPA films and various commercially available ulcer films by lap-shear tests. **g** Comparison of tensile strength of PVA-DOPA films and various commercially available ulcer films by tensile tests. **h** Comparison of interfacial toughness of PVA-DOPA films and various commercially available ulcer films by peel tests. **i** In vivo mucoadhesion of PVA-DOPA films with different content of DOPA after 4 h. White arrow: PVA-DOPA films. Data are presented as the means ± standard deviations (SDs), *P < 0.05; **P < 0.01; ***P < 0.001 vs that of PVA-DOPA1 in **e**, *P < 0.05; **P < 0.01; ***P < 0.001 in **f-h,** one-way ANOVA followed by Tukey's test was used for **e-h**. (n = 3)

Adhesion performances of the PVA-DOPA mucoadhesive film. Mucoadhesive properties of the PVA-DOPA films were determined in terms of residence time and mucoadhesion strength of films on freshly excised porcine buccal mucosa[6,30]. Two methods, the flow-through method and rotating disc method (Supplementary Fig. 2a

and 2b)[6,31], were adopted to investigate the in vitro residence time, which is useful to evaluate whether the film can maintain its adhesion at the buccal mucosa surface for a sufficient time to ensure drug permeation. We evaluated the residence time of PVA-DOPA films by recording the number of remaining films adhered to porcine buccal mucosal. As shown in Supplementary Fig. 2c and 2d, all unmodified PVA films detached from the mucosal surface within 1 hour, thus showing that PVA alone provides only weak adhesion to the buccal mucosa. In contrast, PVA-DOPA films adhered to the buccal tissue for much longer time and especially for PVA-DOPA5 and PVA-DOPA6, nearly all films still stuck to the buccal tissue by the end of 8 h (only recorded up to 8 h for their quick erosion rate).

To evaluate the adhesion strength of the film, we conducted three types of mechanical tests: the shear strength by lap-shear tests (Fig. 2f, Supplementary Movie 1 and 2), the tensile strength by tensile tests (Fig. 2g and Supplementary Movie 3), and the interfacial toughness by peel tests (Fig. 2h and Supplementary Movie 4). We first chose wet porcine buccal mucosal as the model tissue for evaluation of adhesion performance, owing to its close resemblance to human buccal mucosa[32]. The PVA-DOPA film can establish tough and strong mucoadhesion with the wet porcine buccal mucosa upon contact for 10 seconds (Fig. 2f-h). The PVA-DOPA film demonstrated superior adhesion performance compared with tissue adhesives reported in the literature[33,34]. Moreover, the mucoadhesion strength increased with the amount of DOPA, which undoubtedly confirmed that catechol groups can effectively increase mucoadhesion strength, and that such increase was in direct proportion to the content of catechol groups introduced. When compared with existing commercially available ulcer films, including Kanghua Dex Film® (containing vitamin B, dexamethasone, PVA, et al.) (China), Zizhu Propolis Film® (containing propolis cream, glycerin, PVA, povidone, et al.) (China), Yidebang Ulcer Film® (containing chitosan, PVA, et al.) (China), and Curatick® (containing glycerin, PEG, et al.) (Korea). We found that PVA-DOPA1-4 films exhibited comparable or better adhesion performance on wet tissues with these four existing commercial films, while PVA-DOPA5 and PVA-DOPA6 showed significantly superior interfacial toughness, shear and tensile strength than existing commercially available films (Fig. 2f-h) ($P<0.01$). Further in vivo tests also demonstrated that different PVA-DOPA films could stay in touch well with the mucosal tissue of Sprague-Dawley (SD) rats (Fig. 2i) after 4 h. In addition, as depicted in Supplementary Fig. 2e, the PVA-DOPA film also showed self-healing abilities after

hydration, which indicated its potential to autonomously and rapidly heal after breakage in oral environment.

Exploration of the interaction mechanisms between PVA-DOPA film and mucus. The PVA-DOPA film showed a marked adhesion performance on wet buccal tissues. To further disclose the adhesion mechanism of the film, several spectral analyses were performed in an attempt to understand the molecular interactions that occur between the mucosal surfaces and the film. Firstly, the size and zeta-potential of the PVA-DOPA film after mixing with mucin were evaluated. When suspension of mucin particles was mixed with polymers, the mucin particles would aggregate to form larger size if the polymer has a strong affinity to them[35,36]. As shown in Fig. 3a and Supplementary Fig. 3a, all films had a high affinity to mucin particles and the extent of changes in particle size was proportional to the ratio of DOPA. Moreover, the resultant zeta-potential of mucin shifted to higher negative value as a function of time also confirmed the adsorption of PVA or PVA-DOPA molecules on the mucin particles, and that the aggregation tendency depended on the content of DOPA (Fig. 3b).

In addition, we hypothesized that the covalent bonding might occur between the catechol group of PVA-DOPA and thiol groups of mucin and this reaction could be detected by UV-vis absorption spectra[36]. As the results indicated, the UV absorbance increased with increasing DOPA ratios and PVA-DOPA concentrations after mixing with mucin (Fig. 3c and Supplementary Fig. 3b). Therefore, it could be assumed that PVA-DOPA formed catechol-mediated covalent bonding with mucin and lead to a decrease in solubility and thus an increase in the UV-vis absorbance. Comparison of the ^{1}H-NMR spectra of different PVA-DOPA before and after mixing with mucin also verified the formation of covalent bonds between oxidized catechol in DOPA and cysteine-rich domains of glycoprotein in mucin (Supplementary Fig. 3c). In addition, thermodynamic analysis (DSC, differential scanning calorimeter) showed that heat of fusion (ΔH_m) of PVA-DOPA-Mucin blend increased with the increasing ratio of DOPA, as depicted in Supplementary Table 3. This increased trend in ΔH_m value could be attributed to the macromolecular interactions (H-bonds or entanglement of chains) between PVA-DOPA and mucin and the interaction was strengthened with increasing DOPA content. Moreover, SAXS (small-angle X-ray scattering) was also adopted to gain more insights into the interactions between mucin and PVA-DOPA polymer and the potential underlying mechanisms[37]. The scattering profile of PVA-DOPA-Mucin blend became increasingly distinct with increasing DOPA ratio, which demonstrated

that the interactions between PVA-DOPA and mucin was strengthened as DOPA increased, and thus changed the overall conformational state of PVA-DOPA chain, especially at a higher concentration (Fig. 3d).

Therefore, from the results above, it could be speculated that the mucoadhesive property of PVA-DOPA film could be partly attributed to the interpenetration and entanglement of polymer chains with the mucus. Besides physical association, the mucoadhesion of PVA-DOPA film was also due to the formation of hydrogen bonds and covalent bonds between the film and mucin. The phenomenon above also verified the role of catechol groups in mucoadhesion. That is, catechol contains numerous hydroxyl groups that could form hydrogen bonding groups. In addition, the catechol forms quinone quickly upon oxidation, which can further react with amino or thiol groups found in mucus layer, extracellular matrix (ECM) proteins, or carbohydrates of mucus[24,38,39], thus confirming two theories of adhesion: the diffusion theory and the adsorption theory (Fig. 3e).

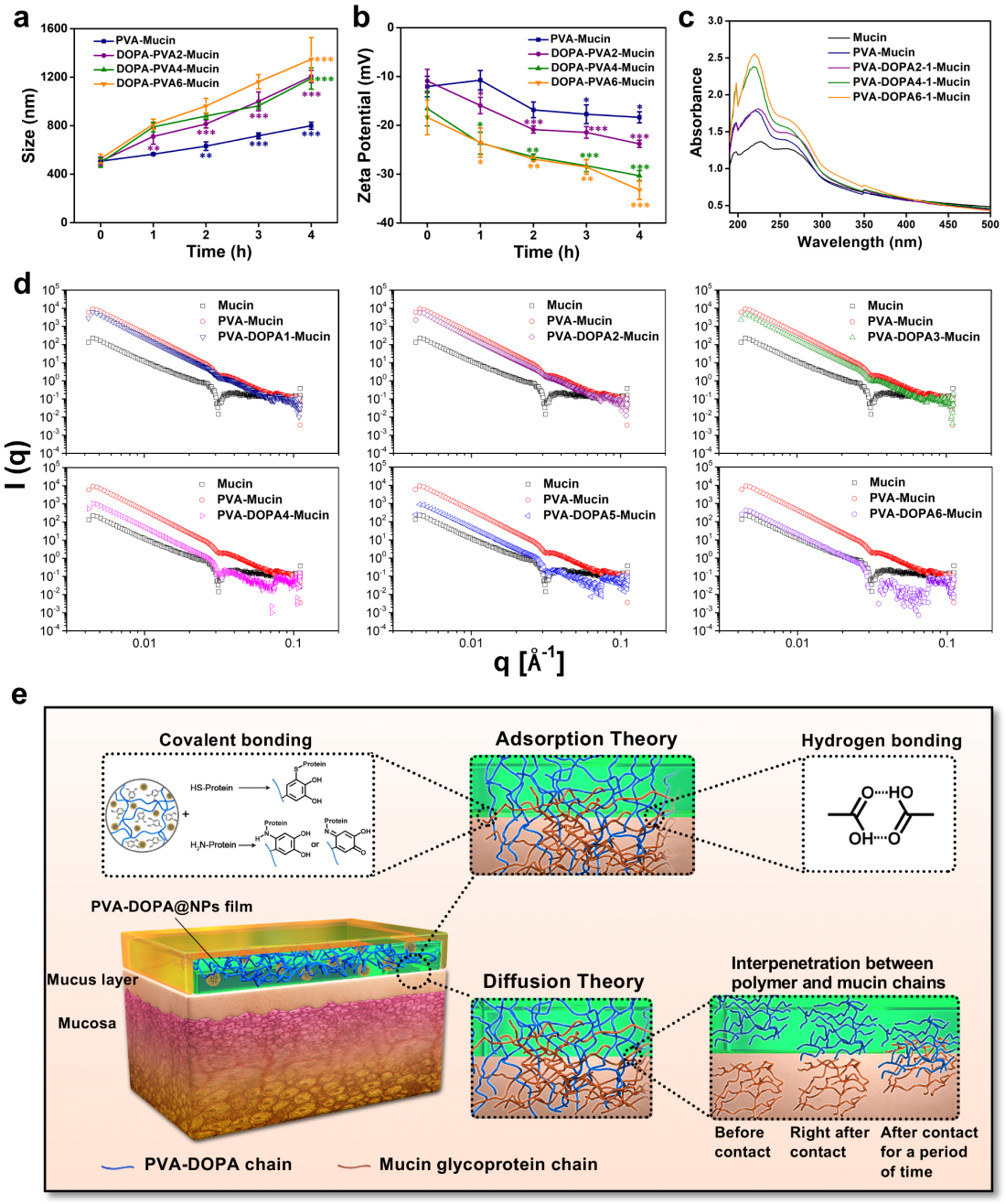

Fig. 3 Interactions of PVA-DOPA films with mucin. a Variation of particle size of different PVA-DOPA-Mucin mixtures as a function of time. **b** Variation of zeta-potential of different PVA-DOPA-Mucin mixtures as a function of time. **c** UV-vis absorbance spectra of different PVA-DOPA-Mucin mixtures. **d** SAXS spectra of different PVA-DOPA-Mucin mixtures. **e** Schematic overview of the interactions between PVA-DOPA film and mucus. Data are presented as the means ± standard deviations (SDs), *P < 0.05; **P < 0.01; ***P < 0.001 vs value at 0 h in **a** and **b,** one-way ANOVA followed by Tukey's test was used for **a and b**. (n = 3)

Synthesis and characterization of modified PLGA NPs. In order to achieve controlled drug release profile, improved mucus-penetrating ability and cellular uptake of the drug delivery system, the bare PLGA cores were modified with PEG, PVA, and PDA, respectively, to obtain the final core-shell PLGA NPs (Fig. 1a). It could be clearly seen in Fig. 4a and Supplementary Fig. 4a-c that the prepared PLGA NPs had uniform

morphology and distribution. In addition, the core-shell structure of PLGA NPs with different surface modifications was shown in transmission electron microscope (TEM) images (Fig. 4b). A PLGA core structure (radius ~200 nm) could be observed in the center, with a dense PEG, PVA, or PDA shell coated on the PLGA nanostructure, respectively. As shown in Supplementary Fig. 4d and 4e, the size of four PLGA NPs was evenly distributed and the average particle sizes were 203.2±12.7 nm, 221.7±15.4 nm, 255.5±11.8 nm, and 242.4±19.0 nm, respectively, as measured by dynamic light scattering (DLS). Additionally, zeta-potential analysis demonstrated that compared to PLGA NPs (-15.4±0.7 mV), PLGA-PEG NPs had a more neutral value of -6.2±1.7 mV, while PLGA-PDA NPs had a more negative surface charges (-24.4±2.8 mV) after PDA coating (Supplementary Fig. 4f) ($P<0.01$). Then surface hydrophobicity of different PLGA NPs was determined using Rose Bengal (RB) adsorption assay and the results showed that modified PLGA NPs had more hydrophilic property, whereas the bare PLGA NPs were slightly more hydrophobic (Supplementary Fig. 4g), likely attributed to the abundant hydroxyl groups introduced after surface modification of PLGA NPs. To conclude, the results above clearly illustrated the successful surface decoration of different PLGA NPs.

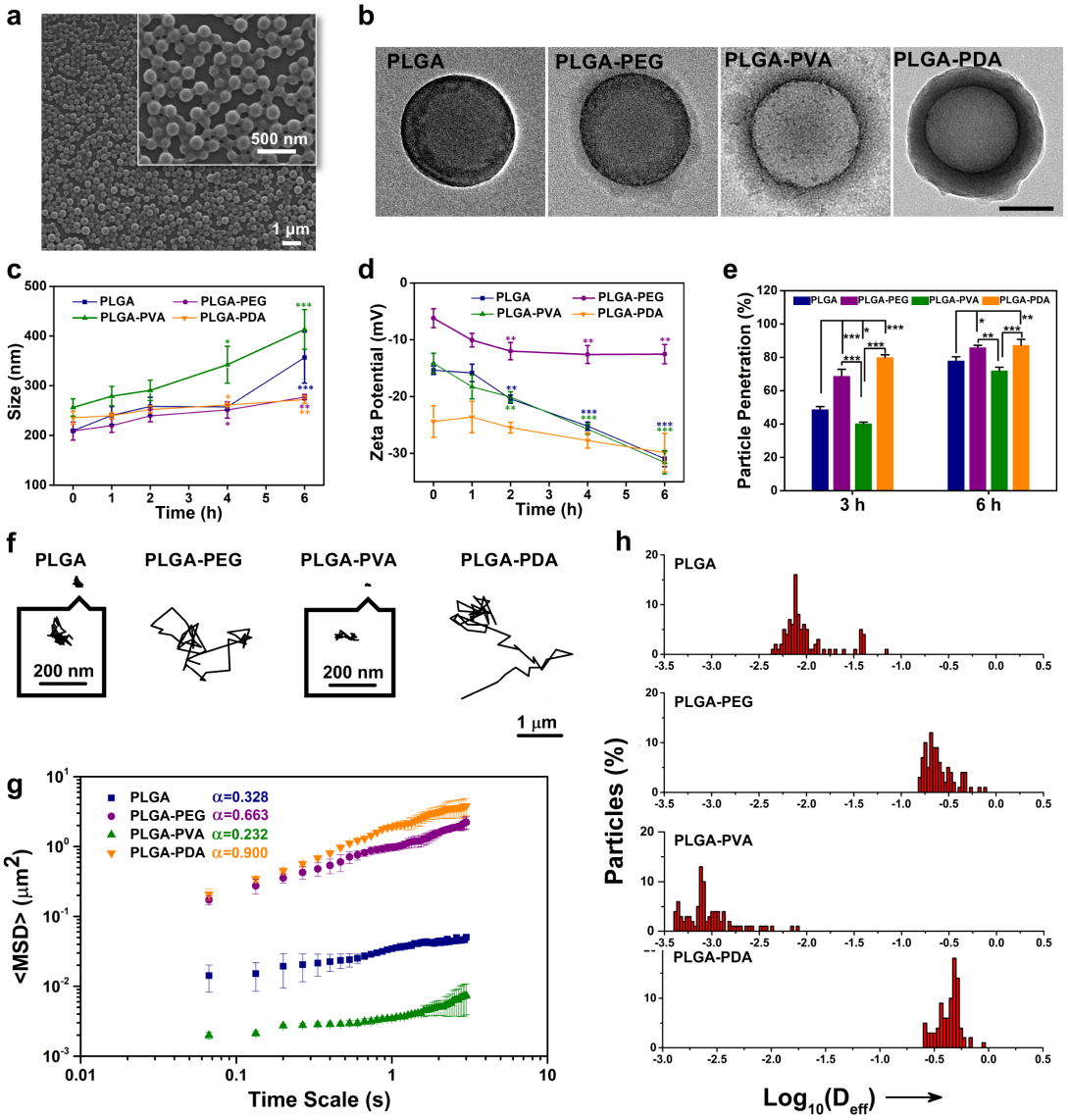

Fig. 4 Characterization and mucus-penetrating properties of NPs in vitro. a SEM image of PLGA NPs. **b** TEM images of PLGA, PLGA-PEG, PLGA-PVA, and PLGA-PDA NPs. **c** Variation of particle size of different NPs-Mucin mixtures as a function of time. **d** Variation of zeta-potential of different NPs-Mucin mixtures as a function of time. **e** Percentage of penetrated NPs across mucus layer in a Transwell assay after 3 h and 6 h. **f** Representative trajectories of different NPs in mucus. **g** <MSD> values as a function of time scale for different NPs in mucus. **h** Distributions of the logarithms of individual particle effective diffusivities (D_{eff}) values at a time scale of 1 s. Data are presented as the means ± standard deviations (SDs), *P < 0.05; **P < 0.01; ***P < 0.001 vs value at 0 h in **c and d**, *P < 0.05; **P < 0.01; ***P < 0.001 in **e**, one-way ANOVA followed by Tukey's test was used for **c-e**. (n = 3)

Mucus-penetrating properties of NPs. After demonstrating the successful synthesis of NPs, the mucus-penetrating ability of different PLGA NPs was investigated. The efficient penetration of NPs through the mucus layer requires minimum interaction between NPs and the mucin particles[40]. Here, we first examined the ability of different NPs to adsorb mucin by probing the variation in average particle size and zeta-potential of NPs[40,41]. When mixed with mucin suspension, bare PLGA and PLGA-PVA NPs

showed a significant larger increase in average size compared with PLGA-PEG and PLGA-PDA NPs (Fig. 4c), indicating much less interaction of PLGA-PEG and PLGA-PDA NPs with the mucin particles. Zeta-potential measurements showed a trend in accordance with particle size, that is, the variations of bare PLGA and PLGA-PVA NPs in zeta-potential were more obvious than that of PLGA-PEG and PLGA-PDA NPs (Fig. 4d), which confirmed that bare PLGA and PLGA-PVA NPs are more likely to bonds with mucin. Likewise, turbidity measurements and mucin absorption percentage were also performed to investigate the interaction between NPs and mucin[41-43] (Supplementary Fig. 5a and 5b), which altogether pointed to the fact that PLGA-PEG and PLGA-PDA NPs interacted much less with mucin than those of bare PLGA and PLGA-PVA NPs.

Then, the ability of different NPs to penetrate through the mucus layer were quantified by using a Transwell system and agarose gel[40,41]. As the results indicated, the bare PLGA and PLGA-PVA NPs that interacted easily with the mucin particles also showed minimal mucus penetration, whereas PLGA-PEG and PLGA-PDA NPs exhibited much higher translocations across the mucus layer (Fig. 4e and Supplementary Fig. 5c). To achieve direct observation of NPs distribution in mucus layer, the diffusion process of NPs was monitored using 3D confocal laser scanning microscopy (CLSM) imaging[44]. Supplementary Fig. 5d represented the z-stacks of different NPs in mucin and as was shown, PLGA-PEG and PLGA-PDA NPs were found in deep layers along the z-direction, while bare PLGA and PLGA-PVA NPs were basically localized in the upper mucus layer, suggesting the potentiality of PLGA-PEG and PLGA-PDA NPs to penetrate through the mucus layer.

To further investigate the behavior of NPs in mucus, the trajectories of particle in mucus were analyzed using a multiple-particle tracking (MPT)[21,40,45]. It was observed that PLGA-PEG and PLGA-PDA NPs were more readily to diffuse across the mucus layer and spanned much larger distances, whereas bare PLGA and PLGA-PVA NPs exhibited highly constrained trajectories (Fig. 4f and Supplementary Movies 5-8). Then the ensemble-averaged mean squared displacement <MSD> for different NPs was quantified and shown in Figure 4g. The rapid mobility of PLGA-PEG and PLGA-PDA NPs were reflected by their <MSD> values being markedly higher across all time scales than those of PLGA and PLGA-PVA NPs. The slope (α) of the <MSD> versus time scale curve on a log-log scale was also calculated to reflect the extent of impediment to particle diffusion (α = 1 indicates unobstructed Brownian diffusion; α < 1 suggests increasing impediment to diffusion as α decreases)[21]. The average α of NPs (Fig. 4g)

was consistent with the Brownian trajectories shown in Fig. 4f and indicated a less hindered motion of PLGA-PEG and PLGA-PDA NPs. We also examined the distribution of the logarithms of individual particle effective diffusivities (D_{eff}) on a time scale of 1 s[45]. As is depicted in Fig. 4h, almost all of the PLGA-PEG and PLGA-PDA NPs exhibited D_{eff} values greater than 0.1 $\mu m^2/s$, indicating rapid diffusion rate across mucus layer. In contrast, few PLGA and PLGA-PVA NPs exceeded that speed.

Cellular transport of NPs in vitro. Besides the mucus layer, the epithelial layer, especially the lipid content of the buccal epithelium, also poses great threat to successful drug delivery[12,46]. Therefore, we next assessed the transport behavior of NPs across epithelia cells. For in vitro evaluation of the cellular uptake of NPs, we adopted the human oral keratinocytes (HOK) and human gingival epithelial cells (HGECs) cell lines originated from human oral mucosa. As shown in Fig. 5a and 5b and Supplementary Fig. 6a and 6b, the PLGA-PDA NPs exhibited the highest cellular internalization among all tested samples in both cell lines. The mean gray intensity level obtained from the fluorescence images also quantitatively confirmed significantly higher cellular uptake of PLGA-PDA NPs compared to other NPs ($P<0.001$) (Fig. 5c and 5d). For further study of cellular internalization and localization of NPs, HOK treated with NPs for 2 h were visualized by TEM images. Notably, the PLGA-PDA NPs showed best cellular uptake capability than other NPs (Fig. 5e) and TEM image also showed that the NPs diffused into the oral mucosa epithelia cells by means of endocytosis (Supplementary Fig. 6c). In addition, an in vitro monolayer model including a mucus layer was developed[47,48]. The TR146 cells was adopted as cell model because they could form an epithelium resembling that of non-keratinized buccal mucosa[49]. A mucus layer was deposited onto the TR146 cell monolayers[47,48]. The TR146 cell monolayer model treated with PLGA-PDA NPs were found most obvious in fluorescent intensity (Fig. 5f and Supplementary Fig. 6d) and the highest percentage of particle penetration across cell monolayer (Fig. 5g), indicating effective permeation ability of PLGA-PDA NPs to transport across the mucus layer and epithelia cells. In contrast, the fluorescent intensity of other three kinds of NPs were much weaker, suggesting decreased cellular internalization.

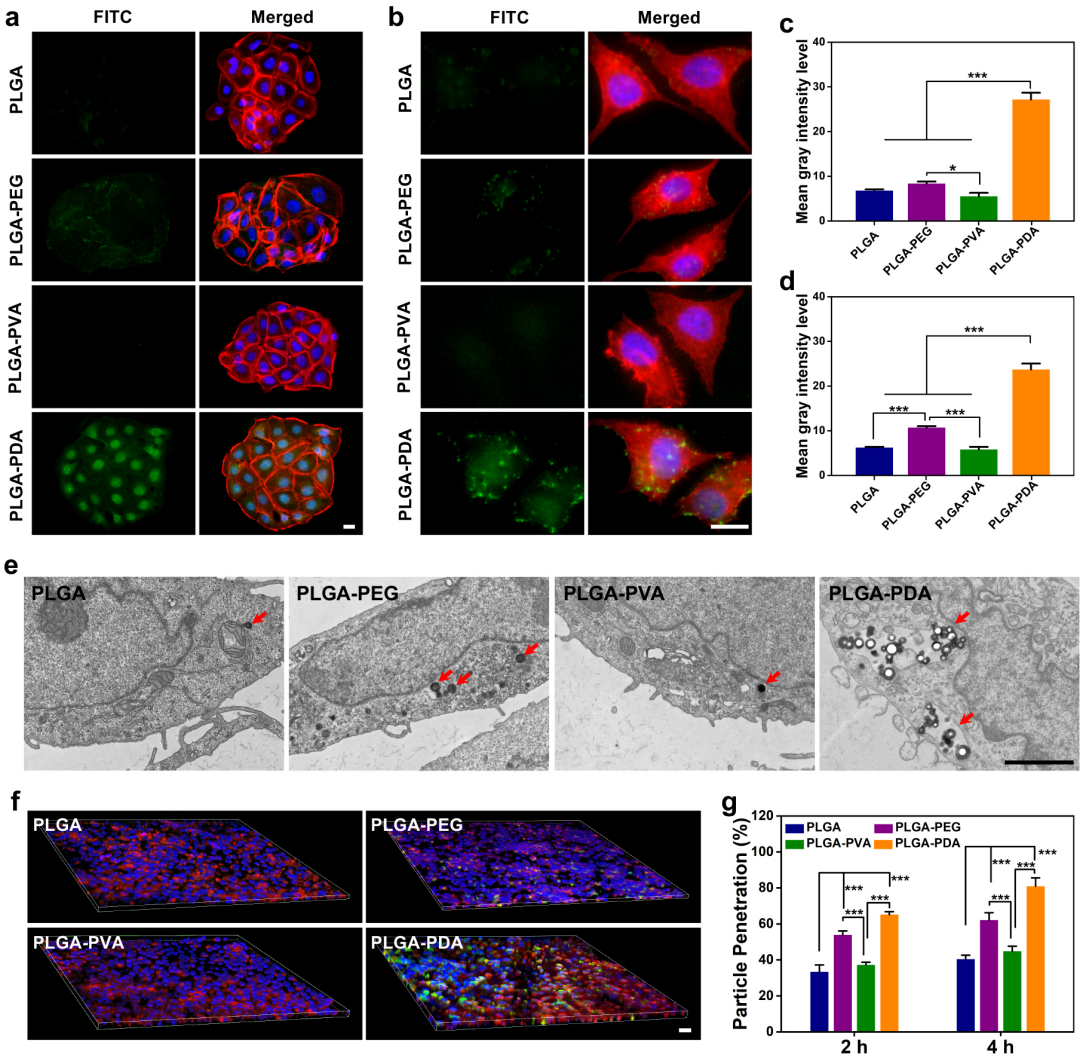

Fig. 5 Cellular uptake of NPs in vitro. a, b Fluorescence image of cellular uptake of different NPs after incubation for 2 h in HOK and HGECs, respectively. Scale bars: 20 μm. **c** Quantification of fluorescence intensity of different NPs obtained from fluorescence image of HOK and HGECs, respectively. **e** TEM images of cellular transport and localization of different NPs in HOK after incubation for 2 h. Scale bar: 2 μm. **f** 3D images of the cellular transport of NPs in the TR146 cell monolayer. Scale bar: 50 μm. **g** Percentage of transported NPs through TR146 monolayer. Data are presented as the means ± standard deviations (SDs), *P < 0.05; ***P < 0.001**,** one-way ANOVA followed by Tukey's test was used for **c, d, and g.** (n = 3)

Fabrication of PVA-DOPA@NPs film and NPs release and entry into tissues ex vivo and in vivo. Next, different PLGA NPs were incorporated into the PVA-DOPA film to form a combined buccal drug delivery system (PVA-DOPA@NPs film). Tensile tests were performed again using fresh porcine buccal mucosa to determine the mucoadhesive properties of films after NPs encapsulation and the results indicated there was no significant difference in mean detachment force between PVA-DOPA and PVA-DOPA@PLGA-PDA NPs films (Supplementary Fig. 7a), which confirmed that NPs incorporation bring no adverse effects to mucoadhesion strength. Additionally, since release of NPs from the film is a primary requisite for its permeation through

mucosa and subsequent drug release, we then investigated the in vitro NPs release analysis from various PVA-DOPA@PLGA-PDA NPs film with different DOPA content. As presented in Supplementary Fig. 7b, PLGA@PDA NPs could release from all kinds of PVA-DOPA@NPs films gradually and the release rate was basically proportional to the amount of DOPA, due to the different erosion rate of various PVA-DOPA films measured before.

Although it has been demonstrated that the PDA modified NPs showed satisfied mucus-penetrating behavior and superior cellular uptake, NPs release from the film and subsequent entry into tissues remains to be investigated. Therefore, we next applied different PVA-DOPA6@NPs films onto the porcine and rat buccal tissue to examine the ex vivo and in vivo efficiency of different NPs entering into mucosal epithelial tissues, respectively. Both the ex vivo and in vivo results confirmed that the PLGA-PDA NPs maintained their superior permeability in terms of transport across epithelium compared with other tested NPs (Fig. 6). Combined together, these results verified the superiority of PDA modified PLGA NPs in epithelia cellular uptake, possibly due to the zwitterionic properties of PDA[50,51], which could not only facilitate mucus penetrating abilities of PDA-coated surfaces, but also cellar transport efficiency.

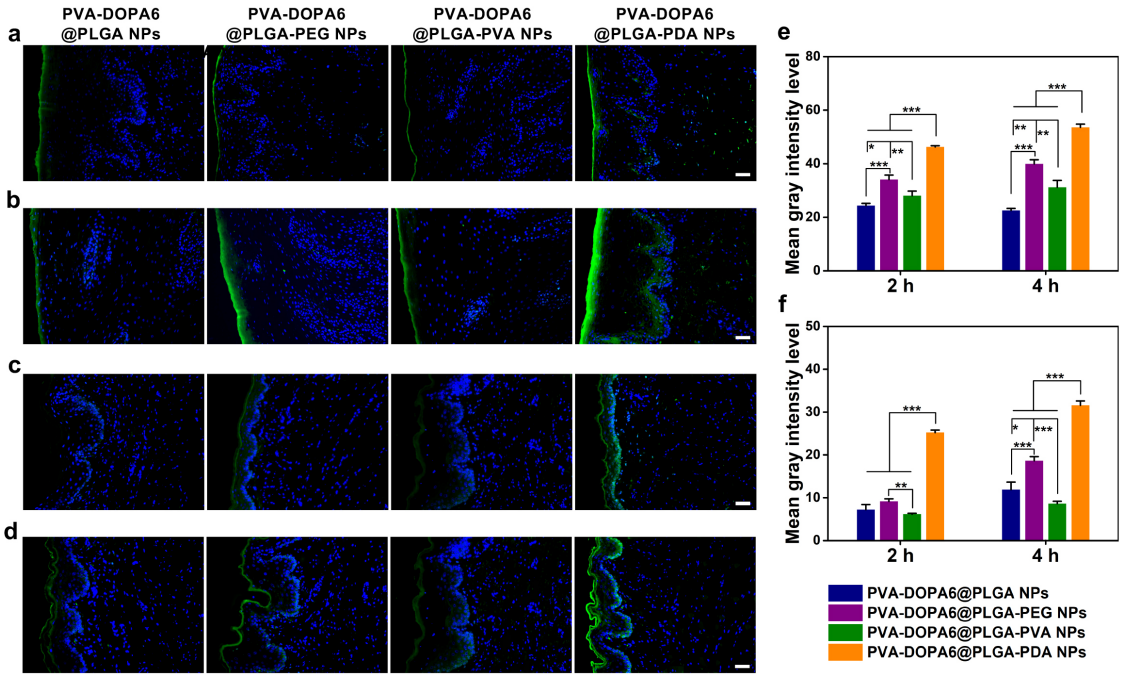

Fig. 6 Permeation studies ex vivo and in vivo. a, b Ex vivo distribution of different NPs in porcine buccal tissue incubated for 2 h and 4 h, respectively. Scale bars: 100 μm. **c, d** In vivo distribution of different NPs in rat buccal tissue incubated for 2 h and 4 h, respectively. Scale bars: 100 μm. **e, f** Quantification of fluorescence intensity of different NPs obtained from fluorescence image of porcine buccal tissue and rat buccal tissue, respectively. Data are presented as the means ± standard deviations (SDs), *P < 0.05; **P < 0.01; ***P < 0.001**,** one-way ANOVA followed by Tukey's test was used for **e and f**. (n = 3)

Toxicity Evaluation of PVA-DOPA@NPs film in vitro and in vivo. Preclinical safety assessment is one of the most important preconditions for drug delivery platform before clinical translation[52,53]. Therefore, a series of toxicity studies, including in vitro cytotoxicity, in vivo histopathology of buccal mucosa and major organs, hematology examination, and biochemical indexes were investigated, respectively (PLGA@PDA NPs were adopted in the toxicity assays)[52,53]. The cytotoxicity of the films was first confirmed using HOK and HGECs cells by CCK-8 assay. The results indicated that cell viability was not affected by film treatment for 1, 2, or 3 days ($P>0.05$) (Supplementary Fig. 8a and 8b), suggesting that the mucoadhesive film were biologically safe. Then the cell attachment analysis was also conducted and detected by fluorescent imaging and SEM. As shown in Supplementary Fig. 8c-f, both HOK and HGECs could grow and proliferate well on the film, thus proving that the PVA-DOPA@NPs films were highly biocompatible.

Apart from in vitro cytotoxicity studies, the in vivo biosafety was further evaluated in SD rats. For the histological analysis, we first evaluated the potential irritation of the films to the buccal mucosa. As a result, Fig. 7a indicated that there were no significant inflammation, necrosis, or metaplasia in the buccal mucosa tissue in contact with the films for 4 h compared with the normal tissue, thus proving high biocompatibility of the film to buccal mucosa. Moreover, further evaluation was performed to detect the histocompatibility of film to major organs (heart, liver, spleen, lung, and kidney). Both morphological observation (Supplementary Fig. 9a) and H&E staining results (Fig. 7b and Supplementary Fig. 9b) showed no obvious tissue damage or pathological change in any of the major organs following film administration for 1 or 7 days. Hematology parameters including the number of red blood cell count (RBC), white blood cell count (WBC), platelet count (PLT), and hemoglobin (HGB) were then detected. As displayed in Fig. 7c-f, there was no significant variation in the experimental group compared to the control group, indicating fine compatibility of the film. Finally, blood biochemistry was performed and the results demonstrated that there was no significant change in the functions of the heart (Mg^{2+}, Ca^{2+}, CK, and LDH-L), liver (ALT and AST) or kidney (BUN and CREA) after 1 or 7 days (Fig. 7g-n). Therefore, all of these toxicity assays demonstrated high biosafety and biocompatibility of the PVA-DOPA@NPs films, indicating its great potential in future clinical translation.

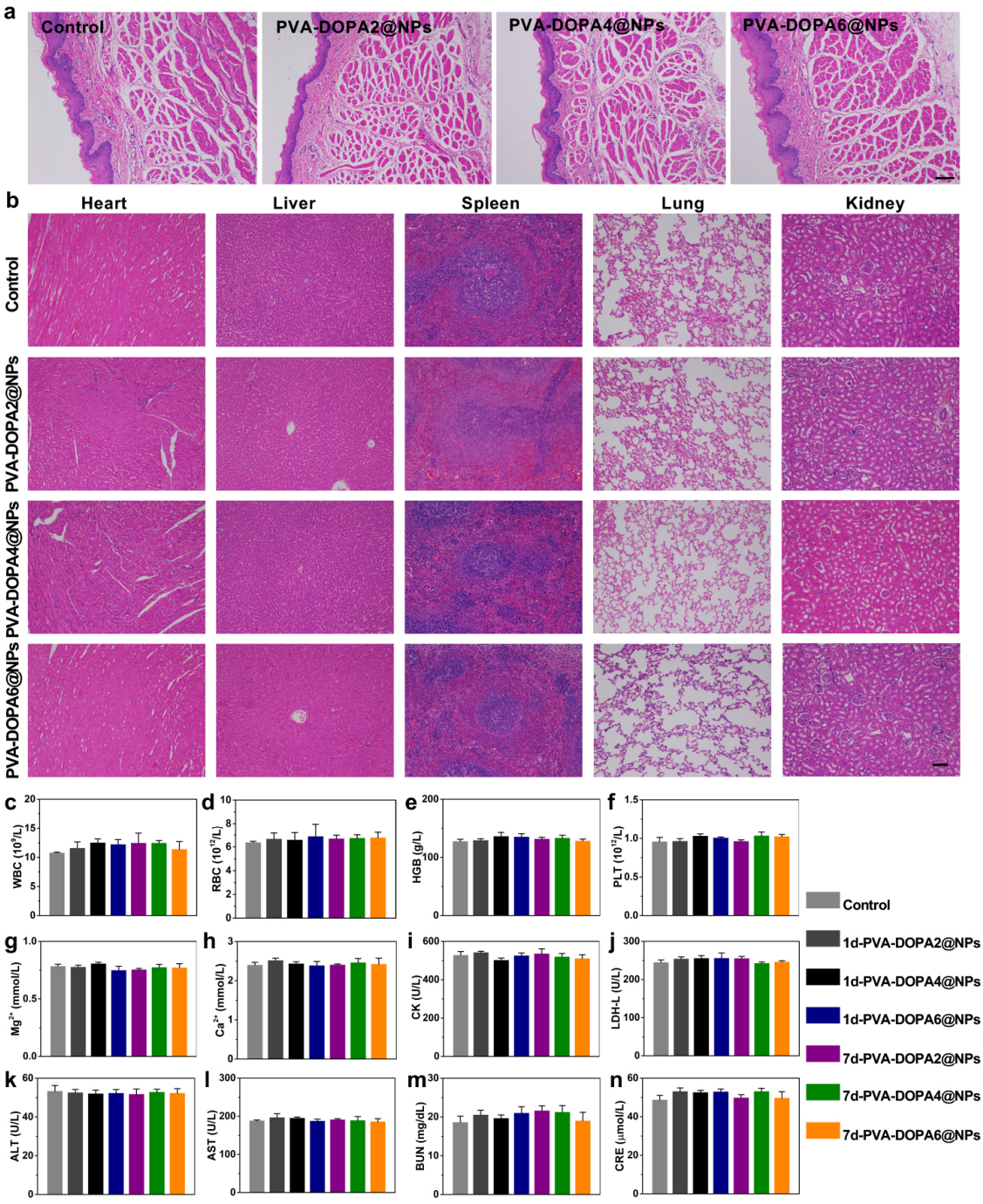

Fig. 7 In vivo biosafety evaluation. a H&E staining of rat buccal mucosa tissue after application of different films for 4 h. Scale bar: 100 μm. **b** H&E staining of major organs (heart, liver, spleen, lung, and kidney) after subcutaneously implanted with different films in the backs of SD rats for 1 day. Scale bar: 100 μm. **c-f** Hematology examination of the variation of WBC (red blood cell count), RBC (white blood cell count), HGB (hemoglobin), and PLT (platelet count) after subcutaneously implanted with different films in the backs of SD rats for 1 or 7 days. **g-n** Blood biochemistry examination of the variation of Mg^{2+}, Ca^{2+}, CK (creatine kinase), LDH-L (lactate dehydrogenase), ALT (alanine transferase), AST (aspartate transferase), BUN (blood urea nitrogen), and CREA (creatinine) after subcutaneously implanted with different films in the backs of SD rats for 1 or 7 days. Data are presented as the means ± standard deviations (SDs). (n = 3)

In vitro drug release and in vivo pharmacokinetic study. In the present study, Dex, a widely used anti-inflammatory drug, was chosen as model compounds to examine the

possibility of the mucoadhesive film for efficient buccal drug delivery[54-56]. The in vitro release behavior of Dex from different PVA-DOPA6@NPs-Dex films was first evaluated. The cumulative percentage of Dex released from NPs impregnated buccal films as a function of time was shown in Supplementary Fig. 10. It was clearly observed that all films with different PLGA NPs achieved a sustained drug release profile. However, film incorporated with PLGA-PDA NPs showed more sustained drug release behavior compared to other three NPs, which might be attributed to the dense PDA coating formed outside the PLGA core (Fig. 4b), hence delaying drug release from NPs and film.

Additionally, having proved that the in vitro release behavior of drug loaded PVA-DOPA@NPs film, we further studied in vivo pharmacokinetics on SD rats. The mean plasma concentration versus time profile of different Dex formulations via oral or buccal routes were depicted in Fig. 8a, and the corresponding pharmacokinetic parameters were listed in Supplementary Table 4. As shown, the pharmacokinetic profiles of Dex were different in both routes. The oral route resulted in high C_{max} at early times, but also decreased rapidly and reached $T_{1/2}$. In contrast, two kinds of buccal therapy provided a lower initial drug concentration but more sustained delivery of Dex from the prepared films, which attained C_{max} in 5.3±2.3 h and 12.0 h and $T_{1/2}$ in 8.9±2.7 h and 20.7±0.7 h, respectively. It was also noticed that the film embedded with PLGA-PDA NPs achieved the highest area under the curve (AUC), which was 3.5-fold, 2.5-fold, and 2.1-fold greater than the values obtained by oral delivered Dox, oral delivered PLGA-PDA NPs, and buccal delivered PVA-DOPA6@PLGA-Dex film, respectively. From the results above, it could be drawn that delivery of drug via buccal application of the mucoadhesive film incorporated with drug-loaded NPs could enhance drug absorption efficiency, possibly due to the direct transmucosal transport of the drug loaded NPs into systemic circulation as against the oral route. In addition, the superior mucus-penetrating and cellular transport abilities of the PDA modified NPs can also improve drug bioavailability, and thus serve as an effective drug delivery nanocarrier.

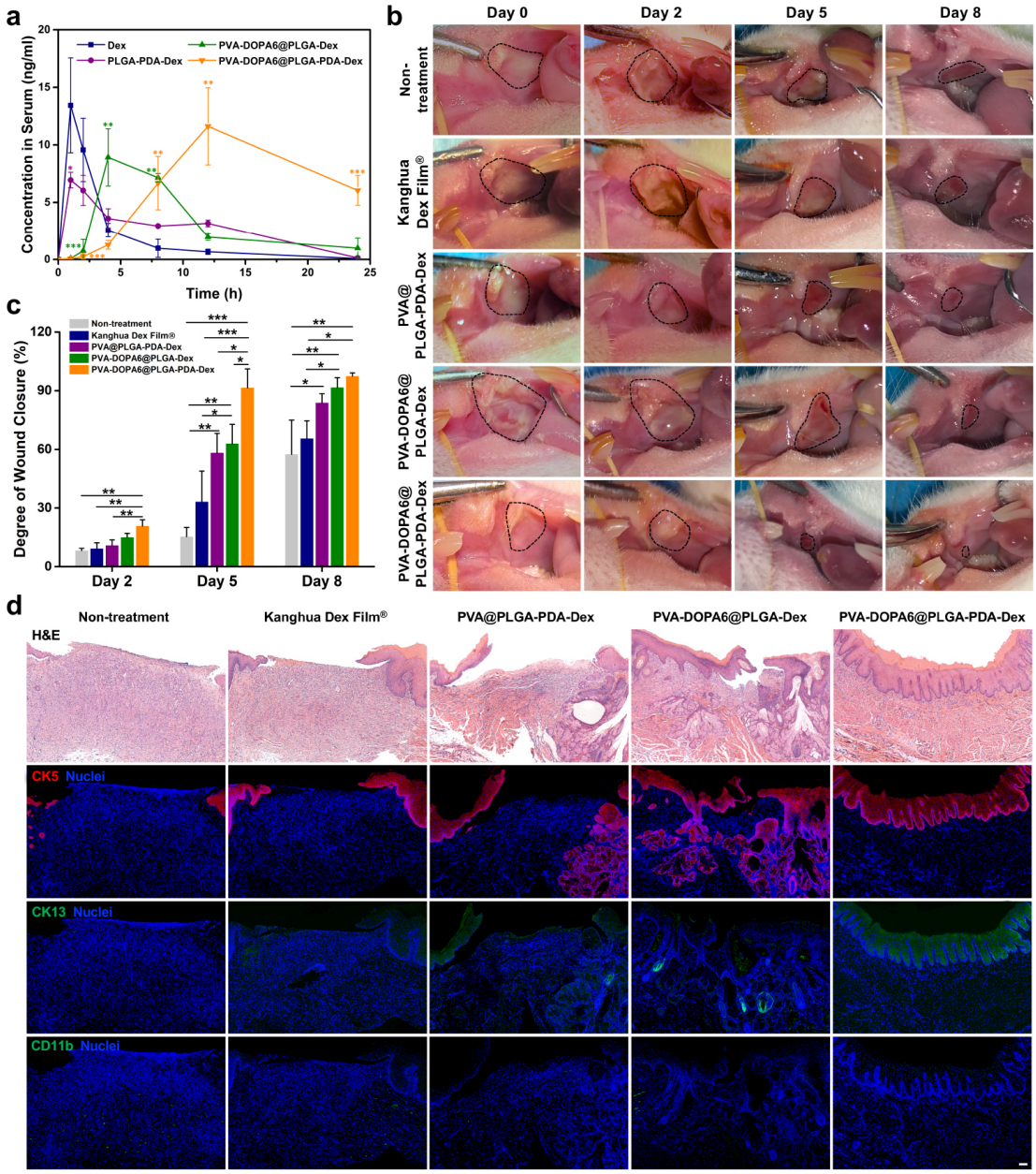

Fig. 8 In vivo pharmacokinetic study and therapeutic efficacy of PVA-DOPA@NPs film in oral ulcer. a Variation of plasma Dex concentration as a function of time after application of different formulations via buccal or oral route. **b** Gross inspection of buccal mucosa ulcers in SD rats treated with Kanghua Dex Film®, PVA@PLGA-PDA-Dex, PVA-DOPA6@PLGA-Dex, PVA-DOPA6@PLGA-PDA-Dex film, and non-treatment at day 0, 2, 5 and 8 (Group 1). **c** Degree of wound closure of the oral ulcers at day 0, 2, 5 and 8. **d** H&E staining and immunohistochemistry staining of anti-keratin5 (CK5, red), anti-keratin13 (CK13, green), and anti-CD11b (CD11b, green) of regenerated oral ulcer at day 8. Nuclei (blue) was stained with DAPI (Group 1). Scale bar: 100 μm. Data are presented as the means ± standard deviations (SDs), *P < 0.05; **P < 0.01; ***P < 0.001 vs that of Dex via oral route in **a**, *P < 0.05; **P < 0.01; ***P < 0.001 in **c**, one-way ANOVA followed by Tukey's test was used for **a and c**. (n = 3)

Therapeutic efficacy of PVA-DOPA@NPs film in vivo. Then we compared the therapeutic effect of a commercial Dex ulcer film with different PVA-DOPA@NPs films loaded with Dex for the treatment of oral ulcers. Severe oral ulcer on buccal mucosa of SD rats was treated with Kanghua Dex Film®, PVA@PLGA-PDA-Dex,

PVA-DOPA6@PLGA-Dex, PVA-DOPA6@PLGA-PDA-Dex film, or non-treatment (n=3, named as Group 1-3 for n=1-3). We observed ulcer sizes for 8 days (Fig. 8b, 8c, Supplementary Fig. 11, and Supplementary Fig. 12). As shown, the three kinds of PVA@NPs/PVA-DOPA@NPs films showed improved therapeutic effect compared with commercial Kanghua Dex Film®. Moreover, PVA-DOPA6@PLGA-PDA-Dex film (91.51±9.63%) was more effective in wound closures at day 5 than PVA@PLGA-PDA-Dex (58.21±9.98%), or PVA-DOPA6@PLGA-Dex (62.95±9.83%) ($P<0.05$), again demonstrating the role of PVA-DOPA in prolonging the residence time of film as well as the ability of PDA modified NPs in continuous delivery of drug.

In histological analysis by H&E staining (Fig. 8d, Supplementary Fig. 13-15), the ulcer treated with PVA-DOPA6@PLGA-PDA-Dex film exhibited completely regenerated epithelium similar to the normal buccal mucosa, whereas there was only partial healing for ulcers treated with other formulations or non-treatment. Moreover, CK5 (expressed at the basal layer where proliferating cells are located) and CK13 (expressed at the intermediate layer and the parabasal layer)[57] immunofluorescent staining showed complete coverage of the epithelium in the PVA-DOPA6@PLGA-PDA-Dex group, whereas coverage was incomplete in other groups (Fig. 8d, Supplementary Fig. 14, and Supplementary Fig. 15). Finally, inflammatory response was evaluated by CD11b staining, the ulcers in all groups showed no obvious $CD11b^+$ cells, demonstrating the biocompatibility of the treated materials (Fig. 8d, Supplementary Fig. 14, and Supplementary Fig. 15).

Discussion

Administration of drug via the buccal route has attracted much attention in recent years and has been used for local and systemic applications. However, several drawbacks have limited its implementation. In this study, we have reported a biologically inspired mucoadhesive film for improved adhesion on buccal mucosal in wet conditions of the oral cavity. This mucoadhesive film offers superb advantages, including strong mucoadhesion strength, high flexibility, and ease of use. Moreover, the DOPA related tunable erosion rate of the PVA-DOPA films makes it potential to be applicable to various kinds of diseases which demand different dosage intervals. Further studies confirmed the role of catechol groups in improved mucoadhesion by forming both covalent and non-covalent bonds with mucin. In addition, our findings may provide new opportunities for the design of tissue adhesives that could also be applied to other wet environments.

Meanwhile, since the use of NPs as drug carriers is a good strategy to overcome the limitations associated with buccal administration route, we incorporated NPs into the mucoadhesive film and explored the ability of different NPs to overcome multiple barriers of buccal mucosa. The results showed that the PDA coated NPs exhibited superior permeability in terms of transport across both mucus layer and epithelia cells compared with other tested NPs, due to the zwitterionic properties of PDA. Furthermore, pharmacokinetic study demonstrated that the mucoadhesive film incorporated with PDA modified NPs showed the best drug bioavailability compared with other buccal film or oral route. In addition, this mucoadhesive film showed improved therapeutic efficacy in treating oral mucositis compared with commercially available ulcer film. Table 1 also summarizes the mucoadhesion strength, transport efficiency across mucosal barriers, drug bioavailability, and therapeutic efficacy of mussel-inspired PVA-DOPA film, demonstrating its superb advantages and potential application to other diseases via buccal route.

In summary, this study presents the design of an effective mussel inspired buccal film with improved residence time and mucoadhesion strength, superior mucus-penetrating and cellular transport abilities, controlled release behavior of drugs, and improved therapeutic efficacy. We anticipate that this platform could improve the efficiency of buccal drug delivery and inspire the rational design of tissue adhesives, wound dressings, and novel NP-based delivery systems in the near future.

Table 1 Summary of mucoadhesion strength, transport efficiency across mucosal barriers, drug bioavailability, and therapeutic efficacy of mussel-inspired PVA-DOPA film

Adhesion strength on wet buccal tissue

Formulations	Lap-shear test (kPa)	Tensile test(kPa)	Peel Test(kPa)
Kanghua Dex Film®	3.78±0.56	2.85±0.93	3.98±1.35
Zizhu Propolis Film®	2.66±0.20	1.94±0.26	1.86±0.37
Yidebang Ulcer Film®	6.15±0.27	4.55±0.47	3.95±1.02
Curatick®	7.64±1.29	5.23±0.99	5.35±0.72
PVA	1.66±0.51	1.50±0.03	1.62±0.49
PVA-DOPA1	3.59±0.14	1.79±0.45	3.53±1.45
PVA-DOPA2	4.42±1.23	2.96±0.87	4.76±0.17
PVA-DOPA3	7.67±4.01	5.49±3.10	5.62±1.48
PVA-DOPA4	11.46±5.54	5.87±1.16	7.83±2.68
PVA-DOPA5	28.81±7.44	12.02±1.43	13.51±2.74
PVA-DOPA6	38.72±10.94	15.60±4.11	15.82±3.93

Transport efficiency across mucosal barriers

Formulations	TR146 cell monolayer model (penetration percentage) (%)	Pig ex vivo model (Mean gray intensity level)	SD rat in vivo model (Mean gray intensity level)
PVA-DOPA6@PLGA	40.37±2.25	22.53±0.79	11.92±1.73
PVA-DOPA6@PLGA-PEG	62.04±4.17	39.93±1.53	18.64±0.94
PVA-DOPA6@PLGA-PVA	44.81±2.80	31.15±2.58	8.64±0.54
PVA-DOPA6@PLGA-PDA	80.93±4.66	53.55±1.2	31.58±1.03

Drug bioavailability

Formulations	T_{max} (h)	$T_{1/2}$ (h)	AUC_{0-24} (ng/ml*h)
Dex	1.00±0.0	2.1±0.2	45.18±11.48
PLGA-PDA-Dex NPs	1.00±0.0	4.1±2.7	64.70±1.52
PVA-DOPA6@PLGA-Dex	5.3±2.3	8.9±2.7	78.12±8.23
PVA-DOPA6@PLGA-PDA-Dex	12.0±0.0	20.7±0.7	160.17±43.86

Therapeutic efficacy

Formulations	Degree of wound closure (%)		
	Day 2	Day 5	Day 8
Non-treatment	8.20±1.20	15.28±4.76	57.44±17.55
Kanghua Dex Film®	9.17±3.05	33.13±15.70	65.46±9.18
PVA@PLGA-PDA-Dex	10.84±2.83	58.21±9.98	83.79±4.68
PVA-DOPA6@PLGA-Dex	14.99±2.03	62.95±9.83	91.66±5.05
PVA-DOPA6@PLGA-PDA-Dex	20.77±3.18	91.51±9.63	97.43±1.70

Data are presented as the means ± standard deviations (SDs). (n = 3). T_{max}, time at which maximum plasma concentration is attained; $T_{1/2}$, elimination half-life; AUC, area under concentration-time curve.

Methods

Materials. Poly(vinyl alcohol) (Mw 85-124 kDa), 3,4-dihydroxy-D-phenylalanine (DOPA), and poly(D,L-lactide-co-glycolide) (PLGA) were purchased from Sigma-Aldrich (USA). Ethyl cellulose, bovine submaxillary mucin, and poly(ethylene glycol) (PEG) were purchased from Shanghai Yuanye Bio-Technology Co., Ltd. (China). Lysozyme, dopamine hydrochloride, FITC, TRITC Phalloidin, DAPI, Dex, Rose Bengal sodium salt, Tris buffer, and agarose were purchased from Beijing Solarbio Science & Technology Co., Ltd. (China). Alexa Fluor-555-WGA was purchased from Thermo Fisher Scientific (USA). Enhanced cell counting kit-8 (CCK-8) was obtained from Saint-Bio Co., Ltd. (China). Anti-cytokeratin5 (CK5, ab52635) was obtained from Abcam (UK), anti-cytokeratin13 (CK13, GB11802) was purchased from Servicebio (China), and anti-CD11b (bs-1014R) was obtained from Bioss (USA).

Cell culture. HGECs cell line was obtained from State Key Laboratory of Oral Diseases, Sichuan University. HOK and TR146 cell lines were purchased from GuangZhou Jennio Biotech Co., Ltd. (China). HOK, HGECs, and TR146 were respectively maintained in minimum Eagle's medium (MEM; Gibco), keratinocyte serum free medium (K-SFM; Thermo Fisher Scientific), and Roswell Park Memorial Institute 1640 medium (RPMI 1640; HyClone), supplemented with 10% (v/v) fetal bovine serum (FBS; Gibco) and 1% penicillin and streptomycin (100 IU/ml) at 37 °C under 5% CO_2.

Animal care. Male Sprague-Dawley rats (250 ± 10 g) were provided by Chengdu Dashuo Bio-Technology Co., Ltd. (China). All experiments involving animals were carried out in compliance with the Institutional Animal Care and Use Committee of Sichuan University, Chengdu, China. Rats were fed with a standard laboratory diet of a 12h/12h light/dark cycle under SPF conditions and had at least one week of acclimatization before any animal experiment.

Synthesis and characterization of PVA-DOPA film. The PVA-DOPA polymers were synthesized according to a previous study[58] and with some modifications. Briefly, PVA (6 mmol) was dissolved in DMSO (30 ml) under 100 °C and 0.75 g $NaHSO_4 \cdot H_2O$ was then added to into the PVA solution. After the temperature decreased to 80 °C, different amounts of DOPA (1-6 mmol) ($n_{(DOPA)}$: $n_{(PVA)}$ =1:6, 1:5, 1:4, 1:3, 1:2, and 1:1) were added, which were represented by PVA-DOPA1, PVA-DOPA2, PVA-DOPA3, PVA-DOPA4, PVA-DOPA5, and PVA-DOPA6, respectively. Then the reaction was kept at 80 °C for 24 h under N_2. After that, the solutions were purified by dialysis for 3 days using a dialysis membrane (MWCO 3,500 Da, Biosharp, China). The final product was freeze dried and stored under vacuum. An ethyl cellulose protective cover was then formed. Briefly, 0.5 ml of 4% ethyl cellulose ethanol solution was added into a 1.5 cm×1.5 cm×1 cm mold and dried under vacuum to form a square open cap with diameter of 1.5 cm and height of 1 mm. The PVA-DOPA film was prepared by pouring 5% w/v PVA-DOPA solutions (PVA-DOPA1-6) into the ethyl cellulose cap mold. Then the mixtures were cured under vacuum at 37 °C. The synthesis of the PVA-DOPA polymers were confirmed by means of FTIR (Thermo Nicolet, USA), UV-vis (SHIMADZU UV-3600, Japan), and ^{1}H-NMR (Bruker DRX, USA) spectroscopy, respectively. The morphology of PVA-DOPA film was observed by SEM (FEI Hillsboro, USA) and the thickness of

the film was measure by digital screw gauge at 5 different locations (n=3). Then the films were immersed in distilled water for 30 min to measure the surface pH of the films using pH test strips. Tensile strength was measured using a universal testing machine (Instron 5567, USA) with a loading speed of 5 mm/min. The rheological properties of the film were characterized by a rotating rheometer (TA Instruments, USA) at 25 °C and frequency sweep (0.01-100 Hz at 0.1 strain) experiment was carried out to examine the storage (G′) and loss (G″) moduli. As for the hydration and degradation tests, the films were weighed (W_0) and immersed into PBS containing lysozyme (0.5% w/v). At regular intervals, films were taken out and weighed (W_1). Then the swollen films were dried under vacuum overnight and weighed again (W_2). The percentage of hydration (Q_H%) was calculated as: $Q_H\%=(W_1-W_0)/W_0\times100$ and the percentage of erosion (Q_E%) was calculated as: $Q_H\%=(W_2-W_0)/W_0\times100$ (n=3).

As for the evaluation of mucoadhesion, the ex-vivo residence time was first assessed by two methods. Fresh porcine buccal tissue obtained from a local slaughterhouse was glued onto a PTFE mold and glass slide and the films were pressed for 10 s to be attached on the mucosal tissue. For the flow-through method, the PTFE mold was adopted and the burette filled with PBS was used to simulate the flow of saliva 0.5 ml/min[5]. For the rotating disc method, the glass slide was placed into a beaker immersed with PBS with a rotating speed of 1000 rpm. At specific time intervals, the number of films that attached on the buccal tissue was recorded (n=6). Then lap shear and tensile strength were measured using a universal testing machine (Instron 5567, USA) with a loading speed of 10 mm/min. Finally, the self-healing property of the film was confirmed by fracture and reformation testing. In brief, the film was hydrated and cut into two pieces and were brought back into contact for 10 s, followed by stretching to observe the self-healing behavior of the film. For the in vivo mucoadhesion analysis, SD rats (250±10 g) were adopted. The rats were fasted overnight with free access to water and were anesthetized by pentobarbital sodium (0.04 mg/kg). Then, different PVA-DOPA films (n=3) were applied to the buccal mucosa of the rats. After administration for 4 h, the state of films adhered on the buccal tissue were observed and recorded.

Exploration of the interactions between PVA-DOPA film and mucus. Bovine submaxillary mucin was dissolved in PBS (1 mg/ml) and sonicated for 30 min. The mucin suspension was then reacted with different PVA-DOPA solutions under 150 rpm at 37 °C. The size and zeta-potential measurements of the mixture were performed after certain period of time using Zetasizer Nano ZS90 (Malvern Instruments, UK) (n=3). The turbidity of the mixtures was measured by a UV spectrophotometer (Thermo MK3, USA) at 600 nm (n=3). The mixtures were examined by UV-vis, SAXS (Xenocs Xeuss 2.0, France), DSC (Mettler Toledo, Switzerland), and ^{1}H-NMR (Bruker DRX, USA) spectroscopy, respectively.

Preparation and characterization of modified PLGA NPs. 40 mg PLGA (Mw 7-17 kDa) was dissolved in 2 ml of acetonitrile and added into 40 ml of 1% PEG or PVA under sonication for 4 h. Then the PLGA-PEG or PLGA-PVA NPs were collected by centrifugation at 12,000 rcf for 20 min, washed 3 times and resuspended in distilled water. The PLGA NPs was synthesized by the same way without the addition of PEG or PVA. To prepare PLGA-PDA NPs, the above prepared PLGA NPs solution was added into an alkaline 0.5 mg/ml dopamine hydrochloride solution (pH 10,

adjusted by Tris buffer) and reacted for 6 h under gentle magnetic stirring. The PLGA-PDA NPs was then collected and purified by centrifugation at 20,000 rcf for 30 min and repeated for 3 times. The fluorescent NPs were fabricated using the same method except for the addition of FITC in acetonitrile at the beginning. The Dex loaded NPs were also synthetized using the same method and the only difference was adding 5 mg Dex together with 40 mg PLGA in the first procedure. Then fabrication and characteristics of NPs were verified using inverted fluorescence microscope (Leica, Germany), SEM, TEM, AFM, and Zetasizer Nano ZS90. The surface hydrophobicity of NPs was evaluated using Rose Bengal (RB) assay. In brief, 200 μl of 1 mg/ml NPs solutions were mixed with 400 μl of 100 μg/ml Rose Bengal solution and were incubated for different time period under magnetic stirring of 1000 rpm at 25 °C. Afterward, the mixtures were centrifuged at 12,000 rcf for 30 min and the supernatant was detected a UV spectrophotometer at 550 nm (n=3). The percentage of NPs interacted with Rose Bengal solution was therefore calculated.

Mucus Permeation Studies. 1 mg/ml mucin suspension were mixed with 1 mg/ml PLGA, PLGA-PEG, PLGA-PVA, and PLGA-PDA NPs and sonicated for different time period. Then the size and zeta-potential measurements of the mixtures were performed using Zetasizer Nano ZS90 and the turbidity was measured by a UV spectrophotometer. The mucin-NP mixtures were then centrifuged at 12,000 rcf for 30 min and the amount of unadsorbed mucin was detected by a UV spectrophotometer at 258 nm. The mixtures were also examined by UV-vis spectroscopy to explore the interactions between the mucin and NPs.

The mucus-penetrating ability of NPs was assessed using a Transwell system (0.4 μm pores, 24-well, Corning, USA). Briefly, 20 μl 10 mg/ml mucin suspension was uniformly deposited on the Transwell insert. 900 μl ultrapure water was placed in the acceptor compartment and 200 μl 1 mg/ml FITC labeled PLGA, PLGA-PEG, PLGA-PVA, and PLGA-PDA NPs were gently added to the donor compartment. The Transwell plate was incubated at 37 °C in a shaker (150 rpm) for 3 h and 6 h. Afterwards, 100 μl solutions were taken out from the acceptor chamber and the percentage of permeated NPs was quantified using a UV spectrophotometer at λ of 490 nm. Likewise, the penetration test was confirmed by another method using agarose gel. In brief, 1 ml of agarose solution (0.3 w/v %) was dissolved at 100 °C, added into vials and hardened at room temperature. 1 ml of mucin suspension was then uniformly placed on the agarose gel and 200 μl 10 mg/ml different NPs solutions were placed on the mucus layer and incubated at 37 °C in a shaker (150 rpm). After 6 h, the NPs and mucin suspension were withdrawn and the agarose gels were rinsed with distilled water 3 times, melted, and measured by UV spectrophotometry at 490 nm. For 3D mucus-penetrating observations, the mucin suspension was stained with Alexa Fluor-555-WGA (10 μg/ml) for 10 min at 37 °C. Then 1 ml stained mucin was deposited onto a confocal dish and placed on a shaker to get equally thick mucus layers. 100 μl 1 mg/ml FITC-labelled NPs were carefully added dropwise onto the mucus layer and incubated for 30 min at 37 °C. Images were taken every 20 μm distance along the z-axis and 3D images were built using a confocal laser scanning microscopy (CLSM, Nikon N-SIM, Japan).

Multi-particle tracking (MPT). Particle transport rates were analyzed by exploring the trajectories of FITC-labeled NPs. Different NPs (10 μl 1 mg/ml) were added to mucin suspension and incubated

for 2 h at 37 °C. At least 3 independent experiments were carried out for each kind of NPs and trajectories of n ≥ 100 particles were performed for each experiment. Movies were captured at a temporal resolution of 66.7 ms for 20 s using Leica fluorescence microscope with a tracking resolution of 10 nm. The trajectories of NPs were then analyzed by ImageJ software. Time-averaged mean square displacement (MSD) was calculated as $MSD = [x(t+\tau)-x(t)]^2+[y(t+\tau)-y(t)]^2$ (x and y represent the NPs coordinates at a certain time and τ denotes the time scale) and effective diffusivities (D_{eff}) was expressed as $D_{eff} = MSD/ (4\tau)$[21,40,45].

Cellular Uptake of NPs. To quantify cellular uptake of different PLGA NPs, HOK and HGECs were seeded onto a 24-well plate at a density of 1×10^5 and incubated for 24 h. Cells were subsequently treated with FITC-labeled NPs (100 μl 1 mg/ml for each well) for 4 h. Then cells were rinsed with PBS for 2-3 times and the F-actin and nuclei were stained with TRITC phalloidin and DAPI, respectively. After three rinses with PBS, the fluorescence intensity was captured by a Leica fluorescence microscope. The intensities of the fluorescence of NPs were quantified using ImageJ software by calculating the mean gray intensity level of each NPs. In addition, the cell uptake efficiency was further confirmed by means of TEM. Briefly, HOK were seeded onto a 6-well plate at a density of 5×10^5 and incubated for 2 days and were then treated with NPs (500 μl 1 mg/ml for each well) for 2 h. Then cells were collected and fixed with 2.5% glutaraldehyde for TEM observation.

Transepithelial Transport Study. Transepithelial transport study of NPs was carried out on the TR146 cells, which were seeded on 12-well Transwell plates (0.4 μm pores, Corning, USA) at a density of 2×10^4 cells/cm^2 and incubated for 27 days, with mediums changed every other day. Transepithelial electrical resistance (TEER) was measured by Millicell ERS-2 electrical resistance meter (Millipore, USA) to monitor the integrity of cell monolayer. Then mucin suspension was deposited onto the TR146 cell layer and the cells were incubated at 37 °C for 24 h. On the day of experiment, cells were washed with HBSS 2-3 times and treated with 100 μl 1 mg/ml of FITC-labeled NPs in HBSS. After incubation for 2 h and 4 h, 100 μl of samples were taken out from the basolateral side and the ratio of transported NPs was detected by a UV spectrophotometer. Subsequently, the cells seeded on apical side were washed 2-3 times with HBSS and stained with TRITC phalloidin and DAPI. The membrane was then removed from the transwell insert, mounted on a slide and observed by CLSM using the z-axial scanning to observe the transport efficiency of different NPs.

Permeation studies ex vivo and in vivo. Then the prepared NPs were mixed with various PVA-DOPA solutions to form the PVA-DOPA@NPs film. The mucoadhesive properties were confirmed again by means of tensile strength testing after incorporated with NPs. Release of FITC-labelled NPs from the films was also analyzed. Briefly, different films with various content of DOPA were placed on the Transwell insert (0.4 μm pores,12-well). 1.5 ml and 1 ml of ultrapure water was added in the acceptor compartment and the donor compartment, respectively. The Transwell plate was then incubated at 37 °C in a shaker (150 rpm) for 12 h. At regular intervals, 100 μl solutions were taken out from the acceptor chamber at certain time points and the number of released NPs from films was quantified using UV spectrophotometer at λ of 490 nm.

Then the transport of NPs across the porcine buccal mucosa was monitored ex vivo. Briefly, films loaded with FITC-labelled NPs were applied to the fresh porcine buccal tissue and were removed after 3 h and 6 h (n=3). The buccal tissues were fixed with 4% paraformaldehyde and sliced, stained with DAPI, and visualized under a fluorescence microscope (Leica, Germany). For quantitative analysis, ImageJ software was adopted to calculate the mean gray intensity level of each sample. Likewise, the in vivo absorption of NPs was investigated using SD rats (250±10 g), which were fasted overnight with free access to water before experiment. The SD rats were anesthetized by pentobarbital sodium (0.04 mg/kg). Subsequently, films loaded with FITC-labelled NPs were administrated to the buccal mucosa of rats (n=3). After application for 2 h and 4 h, rats were sacrificed and the buccal tissue in contact with the film were withdrawn. Then, the films were removed and the tissues were treated like the porcine tissue reported above and observed under Leica fluorescence microscope. The mean gray intensity level of each slice was also examined through ImageJ software.

In vitro cytotoxicity assay. HOK and HGECs were seeded into 24-well plates at a density of 1×10^5 and 1/4 of PVA-DOPA@PLGA-PDA NPs films were added into each well. After co-cultured for the 1, 2, and 3 days, the relative cell viabilities were determined by CCK-8 assay (n=3). The cell attachment of films was also investigated. HOK and HGECs were seeded into 24-well plates deposited with PLGA-PDA NPs incorporated films at a density of 1×10^5. After 24 h, the culture medium was removed and washed 2-3 times with PBS. Then cells were stained with TRITC phalloidin and DAPI or dehydrated with ethyl alcohol and were observed under fluorescence microscope and SEM, respectively.

In vivo biosafety evaluation. The in vivo biocompatibility of films was examined using SD rats (250±10 g). The rats were fasted overnight with free access to water and were anesthetized by pentobarbital sodium (0.04 mg/kg). Films incorporated with PLGA-PDA NPs (n=3) were applied to the buccal mucosa of the rats for 4 h to assess the potential irritation to buccal mucosa. In addition, films were subcutaneously implanted in the backs of SD rats for 1 or 7 days (n=3). Animals were then euthanized and the buccal tissue or major organs (heart, liver, spleen, lung, and kidney) were harvested, embedded in paraffin, sectioned, and stained with hematoxylin and eosin (H&E) for histological analysis. In addition, the blood samples were obtained from the retro-orbital plexus for hematologic and biochemistry analysis.

In vitro drug release. Then, in vitro drug release profile of Dex loaded films were examined. PVA-DOPA6 films containing different NPs-Dex were placed into a dialysis membrane (MWCO 3,500 Da) and were immersed in 50 ml of PBS at 37 °C with magnetic stirring of 100 rpm. At different time point, 1 ml of the solution was taken out and 1 ml of fresh PBS was added. The released Dex concentration with time was detected using UV spectrophotometer at 240 nm (n=3).

In vivo pharmacokinetics study. Male SD (250±10 g) were fasted overnight with free access to water and were randomly divided into four groups (n=3). Group A: Dex was orally administrated; Group B: PLGA-PDA-Dex NPs was orally administrated; Group C: PVA-DOPA6@PLGA-Dex film was applied via buccal route; Group D: PVA-DOPA6@PLGA-PDA-Dex film was applied via buccal route. Rats were anesthetized by pentobarbital sodium (0.04 mg/kg) and all groups were

administrated with a drug dose of 1 mg/kg. After 4 h, the films in group C and group D were removed. Blood samples were collected from the retro-orbital plexus at different time points (1, 2, 4, 8, 12, and 24 h) and were centrifuged at 3000 rpm for 10 min to obtain the plasma. Then the plasma samples collected were analyzed using liquid chromatography-mass spectrometry (LC-MS) (Thermo Fisher Scientific, USA) to measure Dex levels. Pharmacokinetic parameters were calculated using the DAS software (version 2.0).

In vivo therapeutic efficiency. The SD rats (250±10 g) were anesthetized with pentobarbital sodium (0.04 mg/kg) and oral ulcers were induced by placing a round filter paper (5×5 mm) soaked with 70% acetic acid on the buccal mucosa for 3 min. Two days after inducing the oral ulcer (day 0), Kanghua Dex Film®, PVA@PLGA-PDA-Dex, PVA-DOPA6@PLGA-Dex, and PVA-DOPA6@PLGA-PDA-Dex films were applied onto the buccal mucosa ulcer and the rats with non-treatment were set as the blank control group (n=3). The animals were treated with the same procedure after 2, 5, and 8 days of the first dressing and gross observation was observed each time before film application. The animals were sacrificed on day 8 and the buccal mucosa around the ulcer was collected and the samples were harvested for histological and immunohistochemical analysis. CK5 and CK13 were used to evaluate the regeneration of epithelium and the anti-CD11b was adopted to evaluate the recruitment of inflammatory cells according to manufacturer's instructions. The degree of wound closure was calculated as: Degree of wound closure (%) = (Wound area at Day x- Wound area at Day 0)/ Wound area at Day 0×100.

Statistical analysis. Data were presented as the means ± standard deviations (SDs). Data from experiments were analyzed with Origin 9.1. Statistical analysis was performed with statistical software (IBM SPSS Statistics, v22.0; IBM Corp). One-way analysis of variance (ANOVA) was performed to identify differences between groups and one-way ANOVA followed by Tukey post hoc test was adopted for comparisons among multiple groups (*$P < 0.05$; **$P < 0.01$; ***$P < 0.001$).

Data availability

The authors declare that all the relevant data supporting the findings of this study are available within the article and its Supplementary Information files or from the corresponding authors upon reasonable request.

References

1. Macedo, A. S. *et al.* Novel and revisited approaches in nanoparticle systems for buccal drug delivery. *J. Control. Release* **320**, 125-141 (2020).
2. Lamson, N. G., Berger, A., Fein, K. C. & Whitehead, K. A. Anionic nanoparticles enable the oral delivery of proteins by enhancing intestinal permeability. *Nat. Biomed. Eng.* **4**, 84-96 (2020).
3. Panda, B., Subhadarsini, R. & Mallick, S. Biointerfacial phenomena of amlodipine buccomucosal tablets of HPMC matrix system containing polyacrylate polymer/β-cyclodextrin: Correlation of swelling and drug delivery performance. *Expert Opin. Drug Deliv.* **13**, 633-643 (2016).
4. Patel, V. F., Liu, F. & Brown, M. B. Modeling the oral cavity: In vitro and in vivo evaluations of buccal drug delivery systems. *J. Control. Release* **161**, 746-756 (2012).
5. Patel, V. F., Liu, F. & Brown, M. B. Advances in oral transmucosal drug delivery. *J. Control.*

Release **153**, 106-116 (2011).
6. Xu, J., Strandman, S., Zhu, J. X. X., Barralet, J. & Cerruti, M. Genipin-crosslinked catechol-chitosan mucoadhesive hydrogels for buccal drug delivery. *Biomaterials* **37**, 395-404 (2015).
7. Fonseca-Santos, B. & Chorilli, M. An overview of polymeric dosage forms in buccal drug delivery: State of art, design of formulations and their in vivo performance evaluation. *Mater. Sci. Eng. C Mater. Biol. Appl.* **86**, 129-143 (2018).
8. Li, J. *et al.* Tough adhesives for diverse wet surfaces. *Science* **357**, 378-381 (2017).
9. Karp, J. M. A slick and stretchable surgical adhesive. *N. Eng. J. Med.* **377**, 2092-2094 (2017).
10. Rose, S. *et al.* Nanoparticle solutions as adhesives for gels and biological tissues. *Nature* **505**, 382-+ (2014).
11. Yuk, H. *et al.* Dry double-sided tape for adhesion of wet tissues and devices. *Nature* **575**, 169-+ (2019).
12. Anselmo, A. C., Gokarn, Y. & Mitragotri, S. Non-invasive delivery strategies for biologics. *Nat. Rev. Drug Discov.* **18**, 19-40 (2019).
13. Cu, Y. & Saltzman, W. M. Drug delivery stealth particles give mucus the slip. *Nat. Mater.* **8**, 11-13 (2009).
14. Khanvilkar, K., Donovan, M. D. & Flanagan, D. R. Drug transfer through mucus. *Adv. Drug Deliv. Rev.* **48**, 173-193 (2001).
15. Jo, Y. K., Choi, B. H., Kim, C. S. & Cha, H. J. Diatom-inspired silica nanostructure coatings with controllable microroughness using an engineered mussel protein glue to accelerate bone growth on titanium-based implants. *Adv. Mater.* **29** (2017).
16. Hafner, D. *et al.* Mussel-inspired polymer carpets: Direct photografting of polymer brushes on polydopamine nanosheets for controlled cell adhesion. *Adv. Mater.* **28**, 1489-1494 (2016).
17. Jing, X. *et al.* Highly stretchable and biocompatible strain sensors based on mussel-inspired super-adhesive self-healing hydrogels for human motion monitoring. *Acs Appl. Mater. Interfaces* **10**, 20897-20909 (2018).
18. Zhu, W., Peck, Y., Iqbal, J. & Wang, D. A. A novel DOPA-albumin based tissue adhesive for internal medical applications. *Biomaterials* **147**, 99-115 (2017).
19. Lee, B. P., Messersmith, P. B., Israelachvili, J. N. & Waite, J. H. Mussel-inspired adhesives and coatings. *Annu. Rev. Mater. Res.* **41**, 99-132 (2011).
20. Morales, J. O. & Brayden, D. J. Buccal delivery of small molecules and biologics: of mucoadhesive polymers, films, and nanoparticles. *Curr. Opin. Pharmacol.* **36**, 22-28 (2017).
21. Shan, W. *et al.* Overcoming the diffusion barrier of mucus and absorption barrier of epithelium by self-assembled nanoparticles for oral delivery of insulin. *ACS Nano* **9**, 2345-2356 (2015).
22. Shan, W. *et al.* Enhanced oral delivery of protein drugs using zwitterion-functionalized nanoparticles to overcome both the diffusion and absorption barriers. *ACS Appl. Mater. Interfaces* **8**, 25444-25453 (2016).
23. Macedo, A. S. *et al.* Novel and revisited approaches in nanoparticle systems for buccal drug delivery. *J. Control. Release* **320**, 125-141 (2020).
24. Shan, M., Gong, C., Li, B. & Wu, G. A pH, glucose, and dopamine triple-responsive, self-healable adhesive hydrogel formed by phenylborate-catechol complexation. *Polym. Chem.* **8**, 2997-3005 (2017).
25. Postma, A. *et al.* Self-polymerization of dopamine as a versatile and robust technique to prepare polymer capsules. *Chem. Mater.* **21**, 3042-3044 (2009).
26. Watt, A. A. R., Bothma, J. P. & Meredith, P. The supramolecular structure of melanin. *Soft Matter* **5**, 3754-3760 (2009).
27. Yuk, H., Lu, B. Y. & Zhao, X. H. Hydrogel bioelectronics. *Chem. Soc. Rev.* **48**, 1642-1667 (2019).
28. Al-Dhubiab, B. E., Nair, A. B., Kumria, R., Attimarad, M. & Harsha, S. Formulation and evaluation of nano based drug delivery system for the buccal delivery of acyclovir. *Colloids Surf. B Biointerfaces* **136**, 878-884 (2015).
29. Bhattarai, N., Gunn, J. & Zhang, M. Q. Chitosan-based hydrogels for controlled, localized drug delivery. *Adv. Drug Deliv. Rev.* **62**, 83-99 (2010).
30. Freag, M. S., Saleh, W. M. & Abdallah, O. Y. Laminated chitosan-based composite sponges for transmucosal delivery of novel protamine-decorated tripterine phytosomes: Ex-vivo mucopenetration and in-vivo pharmacokinetic assessments. *Carbohydr. Polym.* **188**, 108-120 (2018).
31. Khutoryanskiy, V. V. Advances in mucoadhesion and mucoadhesive polymers. *Macromol. Biosci.* **11**, 748-764 (2011).
32. Sandri, G. *et al.* Histological evaluation of buccal penetration enhancement properties of

chitosan and trimethyl chitosan. *J. Pharm. Pharmacol.* **58**, 1327-1336 (2006).
33. Cencer, M. *et al.* Effect of pH on the rate of curing and bioadhesive properties of dopamine functionalized poly(ethylene glycol) hydrogels. *Biomacromolecules* **15**, 2861-2869 (2014).
34. Liu, Y. *et al.* Injectable dopamine-modified poly(ethylene glycol) nanocomposite hydrogel with enhanced adhesive property and bioactivity. *ACS Appl. Mater. Interfaces* **6**, 16982-16992 (2014).
35. Takeuchi, H. *et al.* Novel mucoadhesion tests for polymers and polymer-coated particles to design optimal mucoadhesive drug delivery systems. *Adv. Drug Deliv. Rev.* **57**, 1583-1594 (2005).
36. Kim, K., Kim, K., Ryu, J. H. & Lee, H. Chitosan-catechol: a polymer with long-lasting mucoadhesive properties. *Biomaterials* **52**, 161-170 (2015).
37. Menchicchi, B. *et al.* Biophysical analysis of the molecular interactions between polysaccharides and mucin. *Biomacromolecules* **16**, 924-935 (2015).
38. Jenkins, C. L., Meredith, H. J. & Wilker, J. J. Molecular weight effects upon the adhesive bonding of a mussel mimetic polymer. *ACS Appl. Mater. Interfaces* **5**, 5091-5096 (2013).
39. Lee, H., Dellatore, S. M., Miller, W. M. & Messersmith, P. B. Mussel-inspired surface chemistry for multifunctional coatings. *Science* **318**, 426-430 (2007).
40. Poinard, B., Kamaluddin, S., Tan, A. Q. Q., Neoh, K. G. & Kah, J. C. Y. Polydopamine coating enhances mucopenetration and cell uptake of nanoparticles. *ACS Appl. Mater. Interfaces* **11**, 4777-4789 (2019).
41. Porsio, B., Craparo, E. F., Mauro, N., Giammona, G. & Cavallaro, G. Mucus and cell-penetrating nanoparticles embedded in nano-into-micro formulations for pulmonary delivery of ivacaftor in patients with cystic fibrosis. *ACS Appl. Mater. Interfaces* **10**, 165-181 (2017).
42. Sunoqrot, S., Hasan, L., Alsadi, A., Hamed, R. & Tarawneh, O. Interactions of mussel-inspired polymeric nanoparticles with gastric mucin: Implications for gastro-retentive drug delivery. *Colloids Surf. B Biointerfaces* **156**, 1-8 (2017).
43. Pontremoli, C., Barbero, N., Viscardi, G. & Visentin, S. Mucin–drugs interaction: The case of theophylline, prednisolone and cephalexin. *Biorg. Med. Chem.* **23**, 6581-6586 (2015).
44. Nafee, N., Forier, K., Braeckmans, K. & Schneider, M. Mucus-penetrating solid lipid nanoparticles for the treatment of cystic fibrosis: Proof of concept, challenges and pitfalls. *Eur. J. Pharm. Biopharm.* **124**, 125-137 (2018).
45. Yu, M. *et al.* Rapid transport of deformation-tuned nanoparticles across biological hydrogels and cellular barriers. *Nat. Commun.* **9**, 2607 (2018).
46. Chen, Y. P. *et al.* Transdermal protein delivery by a coadministered peptide identified via phage display. *Nat. Biotechnol.* **24**, 455-460 (2006).
47. Marxen, E., Mosgaard, M. D., Pedersen, A. M. L. & Jacobsen, J. Mucin dispersions as a model for the oromucosal mucus layer in in vitro and ex vivo buccal permeability studies of small molecules. *Eur. J. Pharm. Biopharm.* **121**, 121-128 (2017).
48. Teubl, B. J. *et al.* The oral cavity as a biological barrier system: Design of an advanced buccal in vitro permeability model. *Eur. J. Pharm. Biopharm.* **84**, 386-393 (2013).
49. Jacobsen, J., Vandeurs, B., Pedersen, M. & Rassing, M. R. TR146 cells grown on filters as a model for human buccal epithelium. 1. Morphology, growth, barrier properties, and permeability. *Int. J. Pharm.* **125**, 165-184 (1995).
50. Liu, Y., Ai, K. & Lu, L. Polydopamine and its derivative materials: Synthesis and promising applications in energy, environmental, and biomedical fields. *Chem. Rev.* **114**, 5057-5115 (2014).
51. Poinard, B. *et al.* Polydopamine nanoparticles enhance drug release for combined photodynamic and photothermal therapy. *ACS Appl. Mater. Interfaces* **10**, 21125-21136 (2018).
52. An, J. *et al.* ROS-augmented and tumor-microenvironment responsive biodegradable nanoplatform for enhancing chemo-sonodynamic therapy. *Biomaterials* **234**, 119761 (2020).
53. Qiao, Y. *et al.* Light-activatable synergistic therapy of drug-resistant bacteria-infected cutaneous chronic wounds and nonhealing keratitis by cupriferous hollow nanoshells. *ACS Nano* **14**, 3299-3315 (2020).
54. Molinaro, R. *et al.* Biomimetic proteolipid vesicles for targeting inflamed tissues. *Nat. Mater.* **15**, 1037-1046 (2016).
55. Xu, X. *et al.* Facile and Versatile strategy for construction of anti-inflammatory and antibacterial surfaces with polydopamine-mediated liposomes releasing dexamethasone and minocycline for potential implant applications. *ACS Appl. Mater. Interfaces* **9**, 43300-43314 (2017).
56. Follmann, H. D. M. *et al.* Multifunctional hybrid aerogels: hyperbranched polymer-trapped

mesoporous silica nanoparticles for sustained and prolonged drug release. *Nanoscale* **10**, 1704-1715 (2018).
57. Ryu, J. H. *et al.* Chitosan oral patches inspired by mussel adhesion. *J. Control. Release* **317**, 57-66 (2020).
58. Shi, D. *et al.* pH-dependent and self-healing properties of mussel modified poly(vinyl alcohol) hydrogels in a metal-free environment. *RSC Adv.* **5**, 82252-82258 (2015).

Acknowledgements

This work was financially supported by the National Natural Science Foundation of China (81970984, 81970985, 81771122, 81701031). We would like to thank Xiaomeng Gao, Siyu Qin, Mingxin Qiao, Yilin Mao for their help.

Author contributions

S.H. and X.P. planned and executed the main experiments, analyzed the data, and wrote the main manuscript. L.D., Z.Z., Y.L., and J.C. performed some experiments and revised the manuscript. T.C. and P.J. analyzed the data and revised the manuscript. Q.W. and J.W. conceived and designed the experiments and revised the manuscript. All authors critically reviewed and approved the manuscript.

Competing interests

The authors declare no competing interests.

Figures

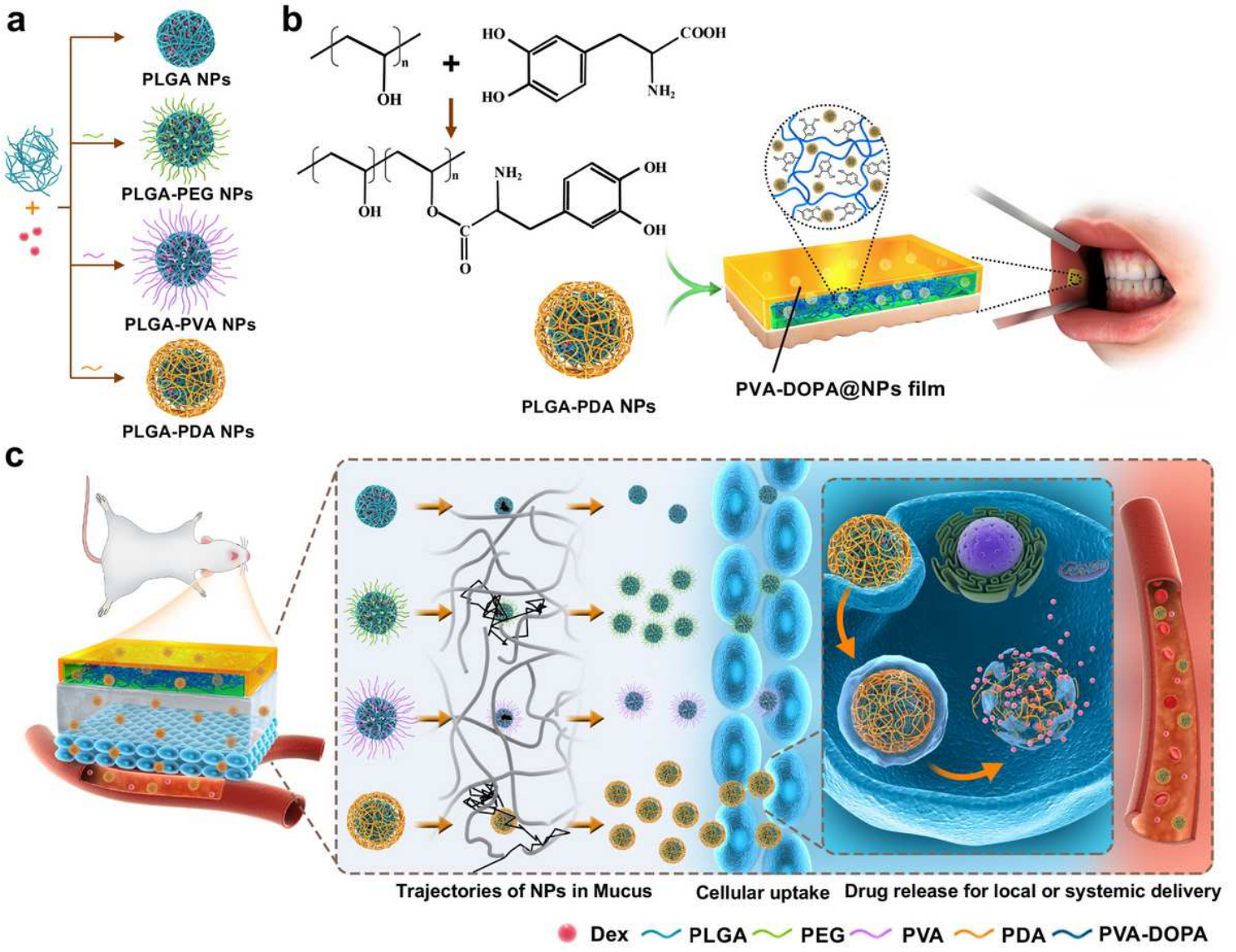

Figure 1

Synthesis and biomedical application of PVA-DOPA@NPs-Dex mucoadhesive film. a Illustrations displaying the method to assemble core-shell PLGA NPs with different surface modifications. b Schematic presentation of fabrication of the PVA-DOPA@NPs-Dex film with enhanced mucoadhesion for buccal drug delivery. c Schematic diagram of application of PVA DOPA@NPs-Dex film on rat buccal mucosa and the process of the NPs to sequentially permeate the mucus layer and the epithelia cells. PDA coated PLGA NPs could overcome both barriers rapidly and subsequently release drug for local or systemic delivery. Dex: dexamethasone, PLGA: poly(lactic-co-glycolic acid), PEG: poly(ethylene glycol), PVA: poly(vinyl alcohol), PDA: polydopamine, DOPA: 3,4-dihydroxy-D-phenylalanine.

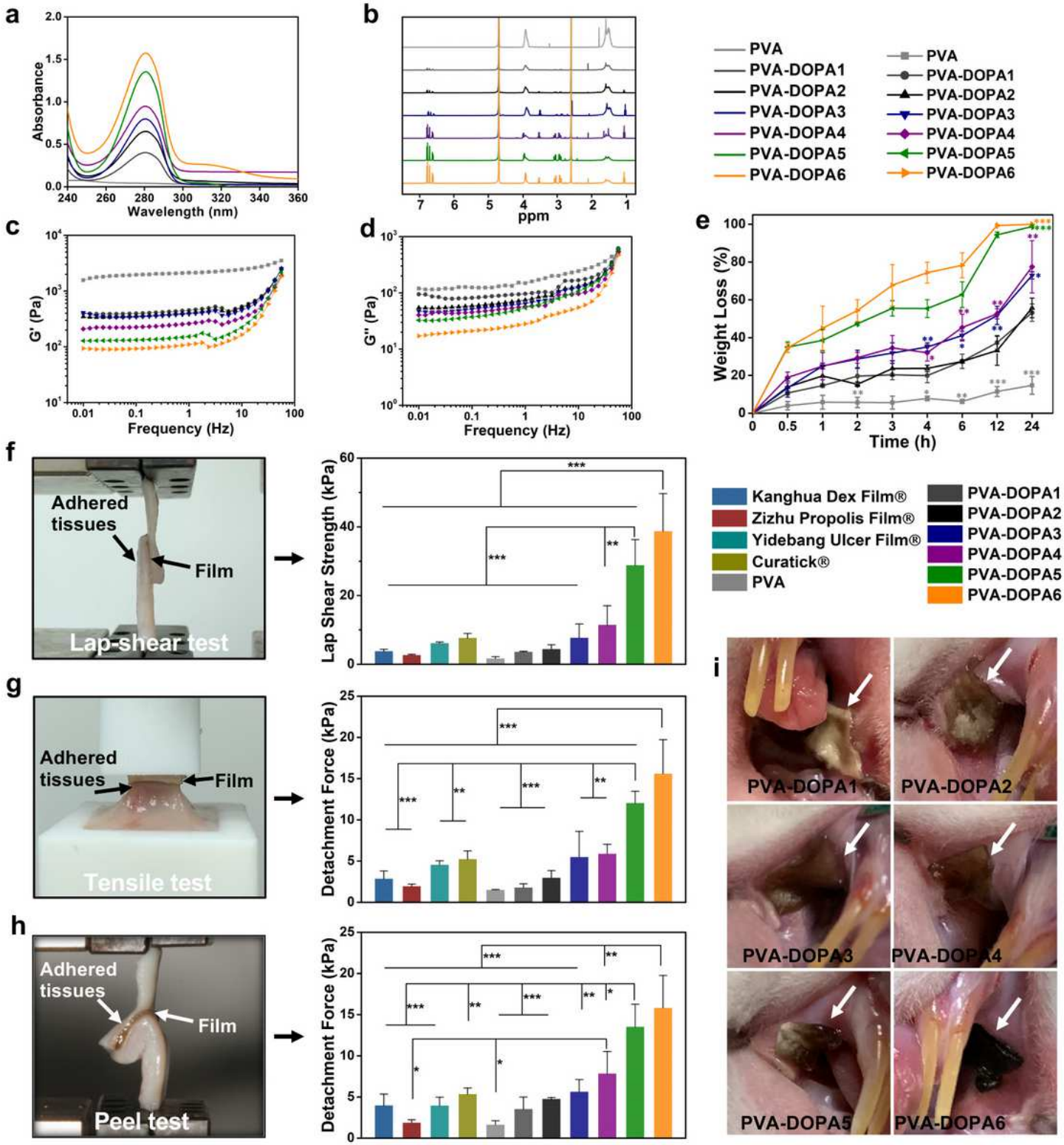

Figure 2

Characterization and adhesion strength of PVA-DOPA films. a UV-vis absorbance spectrum of PVA-DOPA polymers with different amount of DOPA. b 1H-NMR spectra of PVA DOPA polymers with different content of DOPA. c Storage (G') moduli of films with different content of DOPA. d Loss (G") moduli of films with different content of DOPA. e Erosion rate of films with different content of DOPA as a function of time f Comparison of shear strength of PVA DOPA films and various commercially available ulcer films

by lap-shear tests. g Comparison of tensile strength of PVA-DOPA films and various commercially available ulcer films by tensile tests. h Comparison of interfacial toughness of PVA-DOPA films and various commercially available ulcer films by peel tests. i In vivo mucoadhesion of PVA-DOPA films with different content of DOPA after 4 h. White arrow: PVA-DOPA films. Data are presented as the means ± standard deviations (SDs), *P < 0.05; **P < 0.01; ***P < 0.001 vs that of PVA-DOPA1 in e, *P < 0.05; **P < 0.01; ***P < 0.001 in f-h, one-way ANOVA followed by Tukey's test was used for e-h. (n = 3)

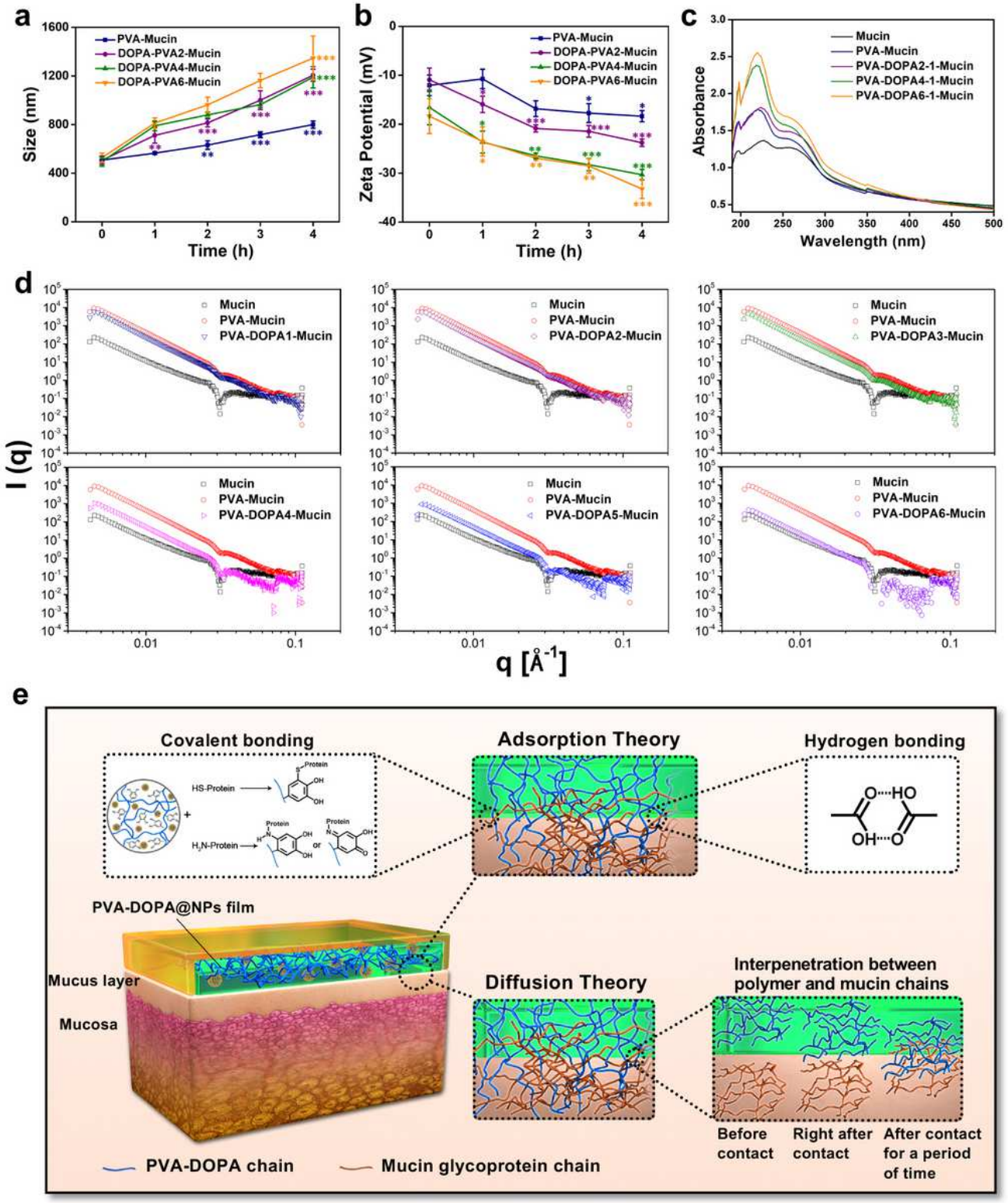

Figure 3

Interactions of PVA-DOPA films with mucin. a Variation of particle size of different PVA DOPA-Mucin mixtures as a function of time. b Variation of zeta-potential of different PVA-DOPA Mucin mixtures as a function of time. c UV-vis absorbance spectra of different PVA-DOPA-Mucin mixtures. d SAXS spectra of different PVA-DOPA-Mucin mixtures. e Schematic overview of the interactions between PVA-DOPA film and mucus. Data are presented as the means ± standard deviations (SDs), *P < 0.05; **P < 0.01; ***P < 0.001 vs value at 0 h in a and b, one-way ANOVA followed by Tukey's test was used for a and b. (n = 3)

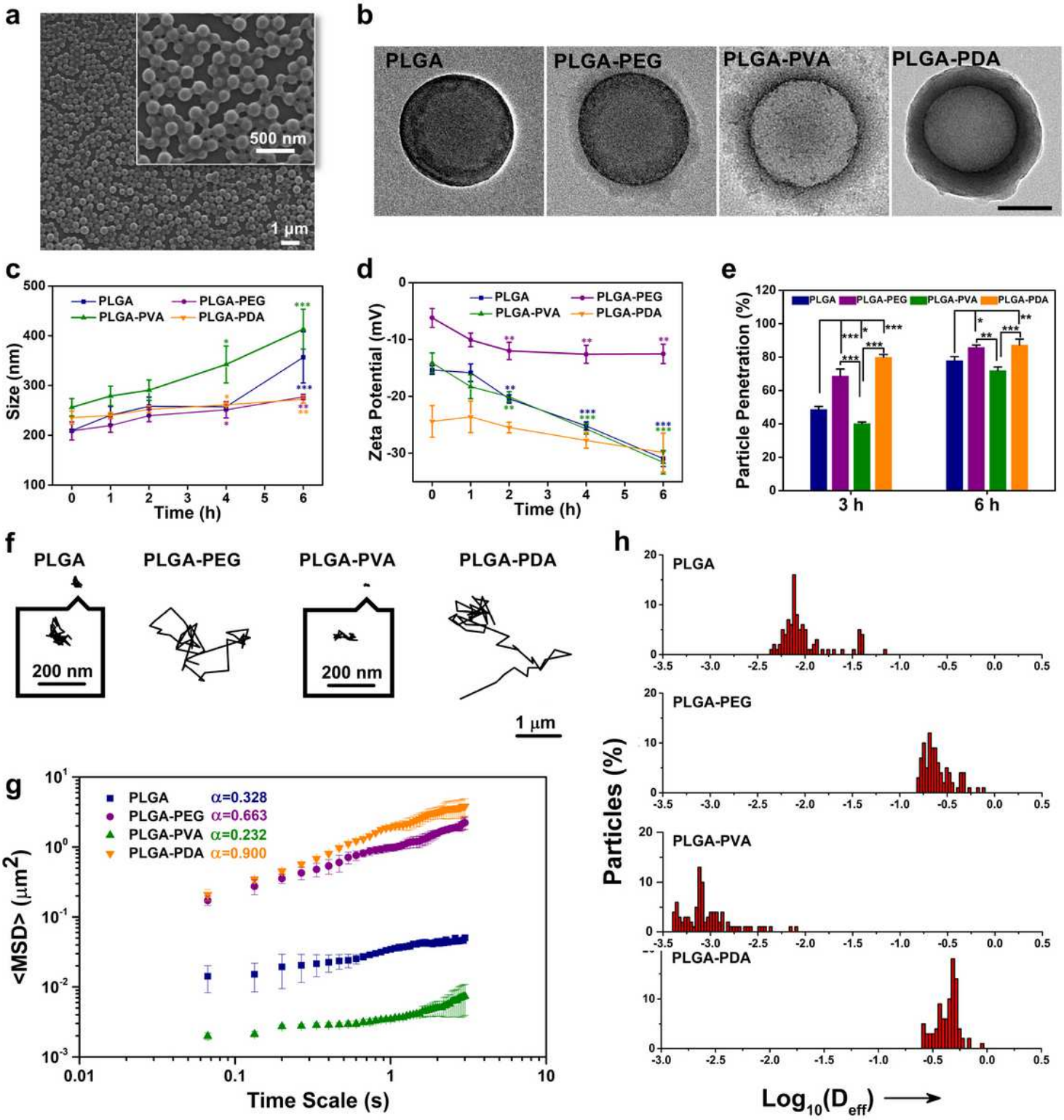

Figure 4

Characterization and mucus-penetrating properties of NPs in vitro. a SEM image of PLGA NPs. b TEM images of PLGA, PLGA-PEG, PLGA-PVA, and PLGA-PDA NPs. c Variation of particle size of different NPs-Mucin mixtures as a function of time. d Variation of zeta-potential of different NPs-Mucin mixtures as a function of time. e Percentage of penetrated NPs across mucus layer in a Transwell assay after 3 h and 6 h. f Representative trajectories of different NPs in mucus. g <MSD> values as a function of time scale for different NPs in mucus. h Distributions of the logarithms of individual particle effective diffusivities (Deff) values at a time scale of 1 s. Data are presented as the means ± standard deviations (SDs), *P < 0.05; **P < 0.01; ***P < 0.001 vs value at 0 h in c and d, *P < 0.05; **P < 0.01; ***P < 0.001 in e, one-way ANOVA followed by Tukey's test was used for c-e. (n = 3)

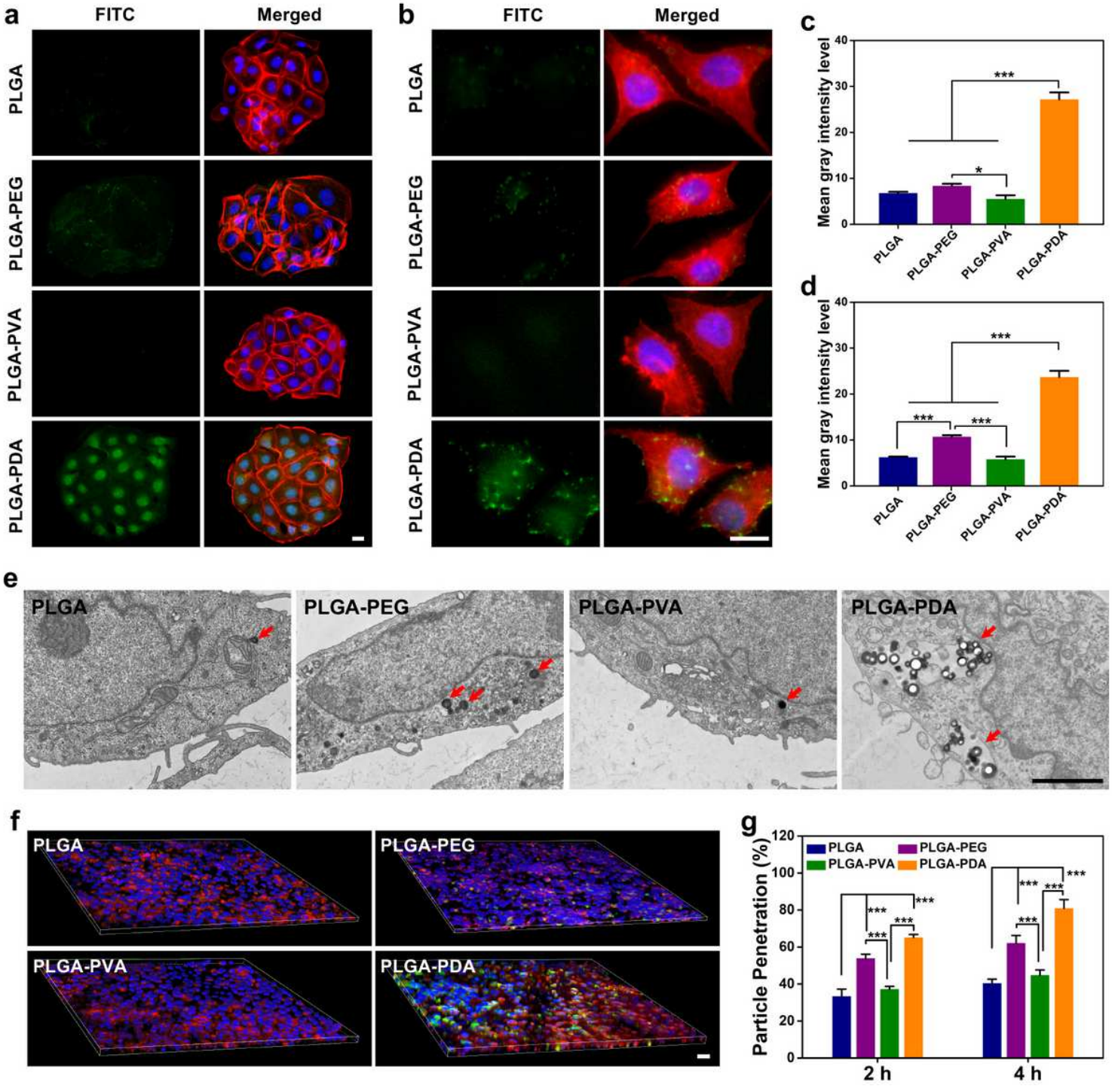

Figure 5

Cellular uptake of NPs in vitro. a, b Fluorescence image of cellular uptake of different NPs after incubation for 2 h in HOK and HGECs, respectively. Scale bars: 20 μm. c Quantification of fluorescence intensity of different NPs obtained from fluorescence image of HOK and HGECs, respectively. e TEM images of cellular transport and localization of different NPs in HOK after incubation for 2 h. Scale bar: 2 μm. f 3D images of the cellular transport of NPs in the TR146 cell monolayer. Scale bar: 50 μm. g Percentage of transported NPs through TR146 monolayer. Data are presented as the means ± standard deviations (SDs), *P < 0.05; ***P < 0.001, one-way ANOVA followed by Tukey's test was used for c, d, and g. (n = 3)

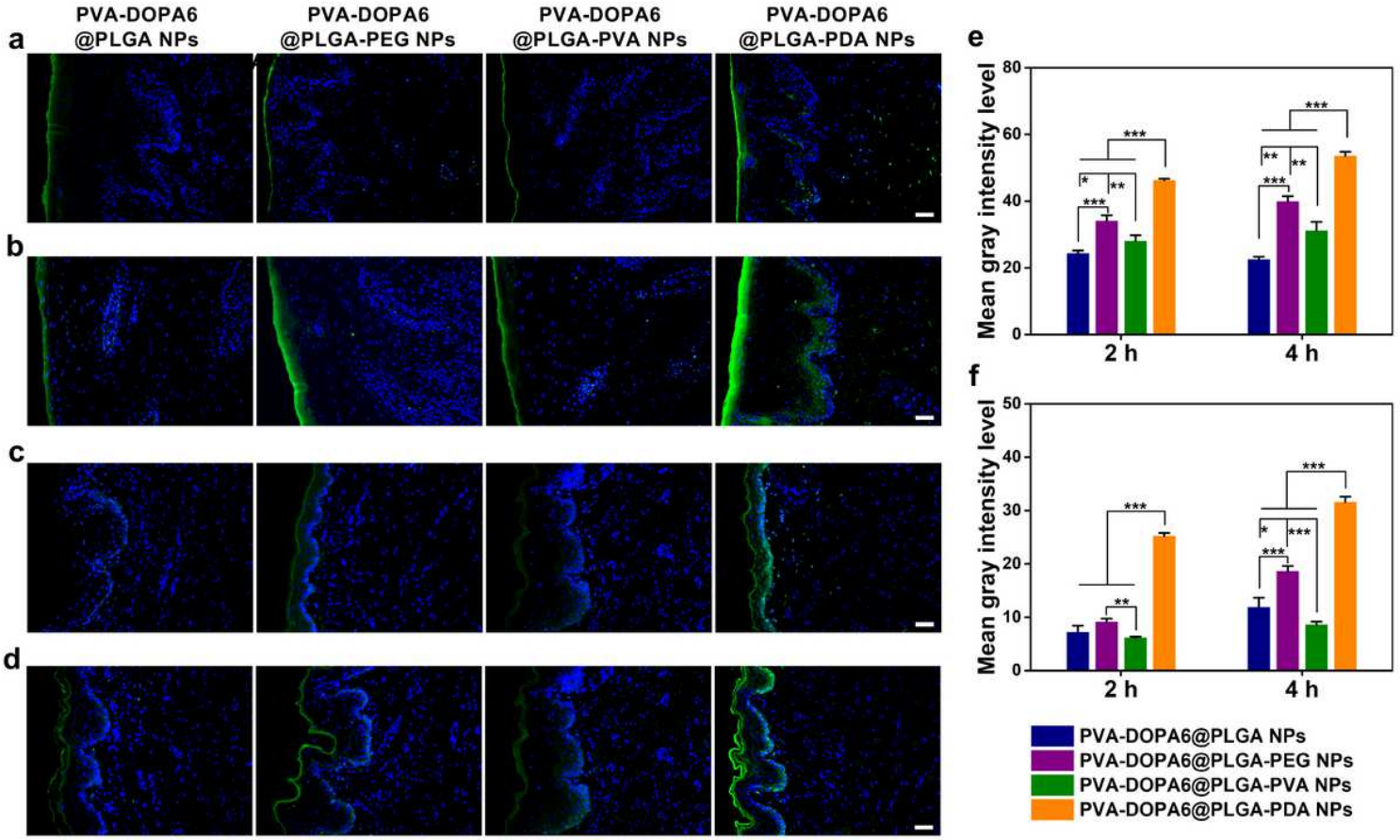

Figure 6

Permeation studies ex vivo and in vivo. a, b Ex vivo distribution of different NPs in porcine buccal tissue incubated for 2 h and 4 h, respectively. Scale bars: 100 μm. c, d In vivo distribution of different NPs in rat buccal tissue incubated for 2 h and 4 h, respectively. Scale bars: 100 μm. e, f Quantification of fluorescence intensity of different NPs obtained from fluorescence image of porcine buccal tissue and rat buccal tissue, respectively. Data are presented as the means ± standard deviations (SDs), *P < 0.05; **P < 0.01; ***P < 0.001, one-way ANOVA followed by Tukey's test was used for e and f. (n = 3)

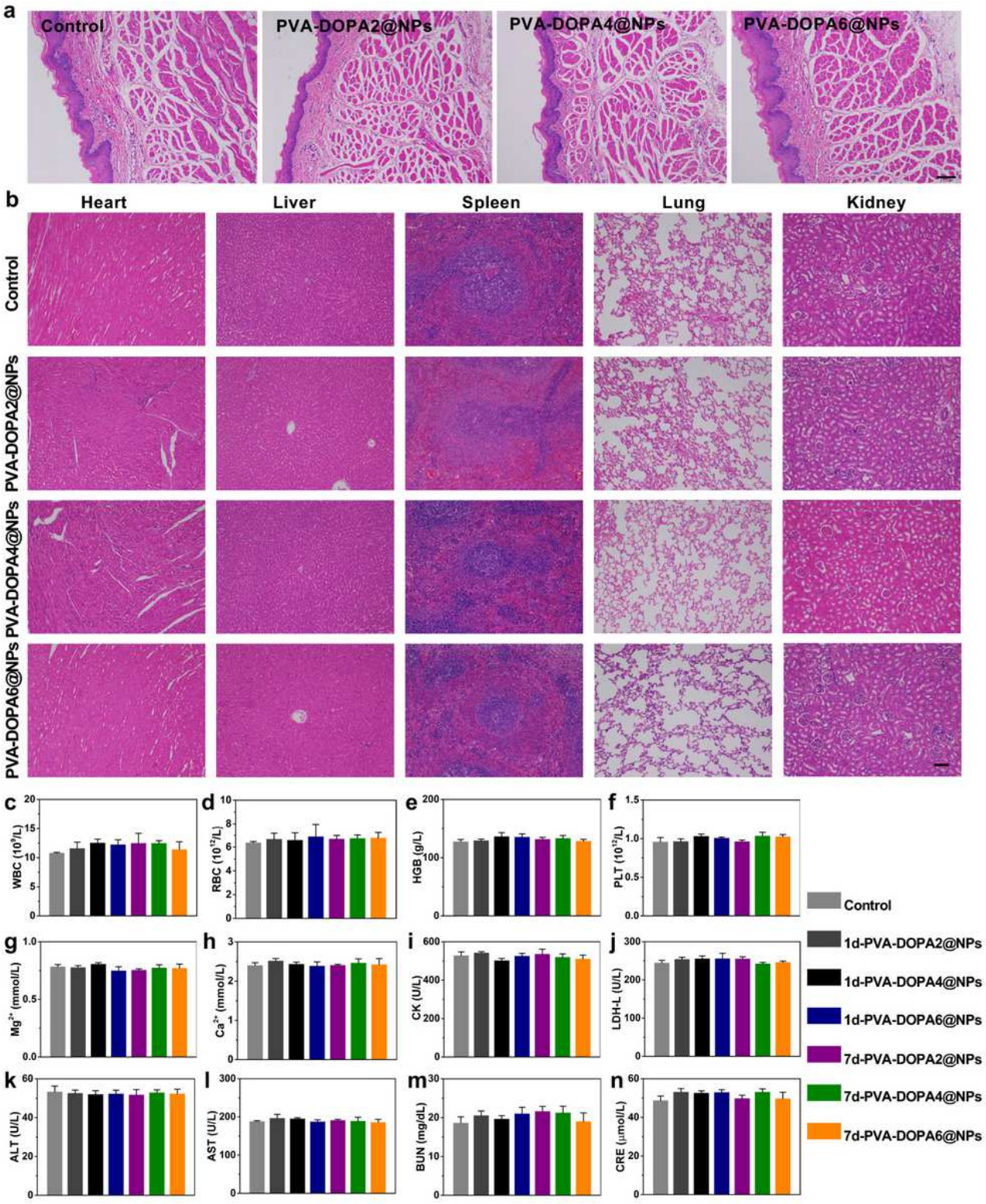

Figure 7

In vivo biosafety evaluation. a H&E staining of rat buccal mucosa tissue after application of different films for 4 h. Scale bar: 100 μm. b H&E staining of major organs (heart, liver, spleen, lung, and kidney) after subcutaneously implanted with different films in the backs of SD rats for 1 day. Scale bar: 100 μm. c-f Hematology examination of the variation of WBC (red blood cell count), RBC (white blood cell count), HGB (hemoglobin), and PLT (platelet count) after subcutaneously implanted with different films in the

backs of SD rats for 1 or 7 days. g-n Blood biochemistry examination of the variation of Mg2+, Ca2+, CK (creatine kinase), LDH-L (lactate dehydrogenase), ALT (alanine transferase), AST (aspartate transferase), BUN (blood urea nitrogen), and CREA (creatinine) after subcutaneously implanted with different films in the backs of SD rats for 1 or 7 days. Data are presented as the means ± standard deviations (SDs). (n = 3)

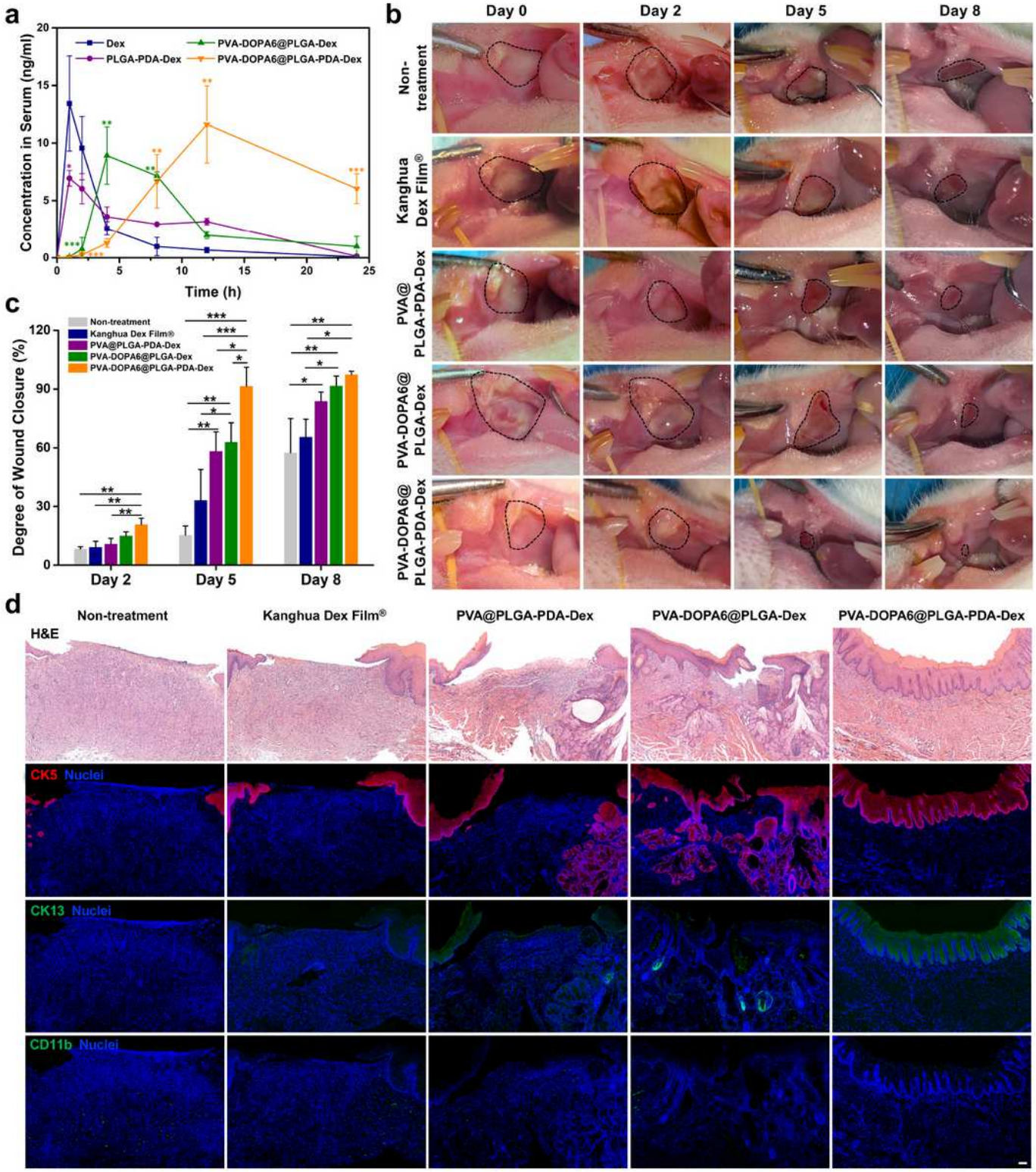

Figure 8

In vivo pharmacokinetic study and therapeutic efficacy of PVA-DOPA@NPs film in oral ulcer. a Variation of plasma Dex concentration as a function of time after application of different formulations via buccal or oral route. b Gross inspection of buccal mucosa ulcers in SD rats treated with Kanghua Dex Film®, PVA@PLGA-PDA-Dex, PVA-DOPA6@PLGA-Dex, PVA DOPA6@PLGA-PDA-Dex film, and non-treatment at day 0, 2, 5 and 8 (Group 1). c Degree of wound closure of the oral ulcers at day 0, 2, 5 and 8. d H&E staining and immunohistochemistry staining of anti-keratin5 (CK5, red), anti-keratin13 (CK13, green), and anti-CD11b (CD11b, green) of regenerated oral ulcer at day 8. Nuclei (blue) was stained with DAPI (Group 1). Scale bar: 100 μm. Data are presented as the means ± standard deviations (SDs), *P < 0.05; **P < 0.01; ***P < 0.001 vs that of Dex via oral route in a, *P < 0.05; **P < 0.01; ***P < 0.001 in c, one-way ANOVA followed by Tukey's test was used for a and c. (n = 3)

Supplementary Files

This is a list of supplementary files associated with this preprint. Click to download.

- SupplementaryMovie1.mp4
- SupplementaryMovie2.mp4
- SupplementaryMovie3.mp4
- SupplementaryMovie4.mp4
- SupplementaryMovie5.mp4
- SupplementaryMovie6.mp4
- SupplementaryMovie7.mp4
- SupplementaryMovie8.mp4
- SupplementaryInformation.pdf